Small-x helicity evolution: An operator treatment

Yuri V. Kovchegov[*]

Department of Physics, The Ohio State University, Columbus, Ohio 43210, USA

Matthew D. Sievert[†]

Theoretical Division, Los Alamos National Laboratory, Los Alamos, New Mexico 87545, USA

We rederive the small-x evolution equations governing quark helicity distribution in a proton using solely an operator-based approach. In our previous works on the subject, the evolution equations were derived using a mix of diagrammatic and operator-based methods. In this work, we rederive the double-logarithmic small-x evolution equations for quark helicity in terms of the "polarized Wilson lines," the operators consisting of light-cone Wilson lines with one or two noneikonal local operator insertions which bring in helicity dependence. For the first time we give explicit and complete expressions for the quark and gluon polarized Wilson line operators, including insertions of both the gluon and quark subeikonal operators. We show that the double-logarithmic small-x evolution of the "polarized dipole amplitude" operators, made out of regular light-cone Wilson lines along with the polarized ones constructed here, reproduces the equations derived in our earlier works. The method we present here can be used as a template for determining the small-x asymptotics of any transverse momentum-dependent (TMD) quark (or gluon) parton distribution functions (PDFs), and is not limited to helicity.

I. INTRODUCTION

Understanding the small-x asymptotics of the quark and gluon helicity distributions is very important for the efforts to resolve the proton spin puzzle: the current measured amounts of the proton's spin carried by its quarks and gluons comes up short of $1/2$, the spin of the proton [1–4]. On the theoretical side, the helicity sum rules [5–7] require the proton spin carried by the quarks and gluons, along with the orbital angular momentum (OAM) of the quarks and gluons, to add up to $1/2$ (see [8] for a review). Therefore, the missing spin could be found either in the less well-known gluon helicity parton distribution function (PDF), in the quark and gluon OAM or in the small Bjorken x region, whose contribution to the proton polarization has not been explored. Indeed, experimental measurements of the double-longitudinal spin asymmetry A_{LL}, which is used to extract the quark and gluon helicity PDFs, are always limited to $x \geq x_{\min}$ with $x_{\min}$ the smallest value of the Bjorken variable x which a given experiment allows to

probe. This way, any given high-energy experiment can never measure the quark and gluon polarizations down to $x = 0$: theoretical input appears to be needed to better constrain the amount of quark and gluon spin at small x, which, in turn, would help us get a better handle on the proton spin puzzle.

In recent years, evolution equations describing the quark and gluon helicity distributions at small Bjorken x have been derived in [9–13] (see also [14,15] for earlier calculations based on a different method). These evolution equations were solved in the large-N_c limit (with N_c the number of quark colors), leading to the following x dependence for the quark and gluon helicity PDFs [10,12,13] in that limit and at perturbatively small values of the strong coupling constant α_s (such that the 't Hooft coupling is small, $\alpha_s N_c \ll 1$):

$$\Delta q(x, Q^2) \sim \left(\frac{1}{x}\right)^{\frac{4}{\sqrt{3}}\sqrt{\frac{\alpha_s N_c}{2\pi}}}, \quad \Delta G(x, Q^2) \sim \left(\frac{1}{x}\right)^{\frac{13}{4\sqrt{3}}\sqrt{\frac{\alpha_s N_c}{2\pi}}}.$$

$$(1)$$

[*]kovchegov.1@osu.edu
[†]sievertmd@lanl.gov

The resummation parameter in the equations derived and studied in [9–13] was $\alpha_s \ln^2(1/x)$. We will refer to the resummation of this parameter as the double logarithmic approximation (DLA). This parameter, originally introduced by Kirschner and Lipatov [16], arises in certain types of small-x evolution describing e.g., polarization or baryon

number transfer from larger to smaller x [16–22]. This parameter does not exist in the more familiar Balitsky-Fadin-Kuraev-Lipatov (BFKL) [23,24] small-x evolution for the unpolarized gluon distribution, which at the leading order resums powers of $\alpha_s \ln(1/x)$.

The helicity evolution equations of [9–13] were written in the s-channel evolution formalism previously used to derive the unpolarized Balitsky-Kovchegov (BK) [25–28] and Jalilian-Marian-Iancu-McLerran-Weigert-Leonidov-Kovner (JIMWLK) [29–32] evolution equations. The helicity evolution was written in terms of the so-called quark or gluon "polarized Wilson lines," which were defined originally in [9] as part of the scattering amplitude of a longitudinally polarized quark or gluon (projectile) on a longitudinally polarized proton (target) which is proportional to the product of the projectile and target polarizations. The operator describing the quark helicity was shown to be related to the "polarized dipole amplitude": the polarization-dependent part of the scattering amplitude for a color-singlet quark–antiquark pair. The polarized dipole amplitude was shown to be a correlation function of a trace of polarized and regular light-cone Wilson lines. Similar to the case of the unpolarized Balitsky hierarchy [25,26], the helicity evolution equations do not close in general. Closed equations were obtained in the large-N_c and the large-N_c and N_f limits [9] (with N_f the number of quark flavors). The large-N_c equations for quark helicity were solved in [10,12] ultimately leading to the Δq small-x asymptotics shown in Eq. (1). Gluon helicity distribution was studied in [13]: new relevant operators had to be defined (see also [33]), their evolution equations were constructed and solved in the large-N_c limit, leading to the small-x asymptotics for ΔG also shown in Eq. (1).

However, an explicit form of the polarized Wilson line operators was not derived in [9–12]. In [13], the first expression for the polarized *quark* Wilson line was written down. It is given below in Eq. (44), and consists of two semi-infinite light-cone Wilson lines, with a subeikonal component F^{12} of the gluon field strength tensor $F^{\mu\nu}$ sandwiched between them. (This F^{12} insertion can be interpreted as arising from $\vec{\mu} \cdot \vec{B} = \mu_z B_z = -\mu_z F^{12}$, where a quark with the chromomagnetic dipole moment $\vec{\mu}$ is traveling through the chromomagnetic background field $\vec{B}$.[1]) We see that helicity dependence enters as a subeikonal operator insertion between the eikonal Wilson lines. This structure of subeikonal corrections at small and large x was also obtained in [34–36]. However, the expression (44) corresponds only to a (subeikonal) gluon exchange with the target shown in the left panel of Fig. 5. An important quark exchange contribution, shown in the right panel of Fig. 5, was missing, as it was not needed in the large-N_c limit largely utilized in [13]. In

addition, the polarized *gluon* Wilson line has never been constructed explicitly.

Our aim here is to rederive the results of [9] for the quark helicity while working entirely in the operator language. That is, we want to construct explicit complete expressions for the quark and gluon polarized Wilson line operators. We then want to "evolve" these operators toward small x, obtaining helicity evolution equations. The benefits of such a calculation are twofold: on the one hand, we would be able to cross-check the results of [9–13]. On the other hand, the operator formalism we are going to develop here can be similarly applied to other TMDs, such as transversity or the Sivers function, to study their small-x asymptotics. Knowing the small-x behavior of various TMDs has a number of useful phenomenological and theoretical implications. Our present work opens the possibility to systematically derive the small-x asymptotics for all the TMDs in the framework of perturbative quantum chromodynamics (QCD), complementing the efforts in [37–42]. In [43] we will apply this formalism to study the small-x asymptotics of the quark transversity TMD.

The paper is structured as follows. In Sec. II we will start with the operator definition of the quark helicity TMD and evaluate it for small x, obtaining the expression (31) relating it to the polarized quark dipole amplitude. The expression we obtain is identical to the one used in [9–11]; however, in [9] it was derived by calculating the cross section for the semi-inclusive deep inelastic scattering (SIDIS). Relating the SIDIS cross section to the quark helicity TMD at the leading order in the coupling we read off the quark helicity TMD in [9]. The calculation in Sec. II provides an independent cross-check of this result and shows that the SIDIS definition of the quark helicity TMD used in [9] is equivalent to the standard operator definition of the same quantity.

Explicit operator expressions for the polarized quark and gluon Wilson lines are constructed respectively in Secs. III A and III B. The results are given by Eq. (51) for the quarks and by Eq. (64) for the gluons. We proceed by constructing the large-N_c evolution equations for "polarized dipoles" in Sec. IV and the large-N_c and N_f evolution equations in Sec. V. The equations are identical to those derived originally in [9].

We conclude in Sec. VI by summarizing our main results and outlining future research directions in this area.

II. QUARK AND GLUON HELICITY TMDS AT SMALL x

A. Quark helicity TMD

We start with the quark helicity TMD defined by [44]

$$g_{1L}^q(x, k_T^2) = \frac{1}{(2\pi)^3} \frac{1}{2} \sum_{S_L} S_L \int d^2r \, dr^- e^{ik \cdot r} \langle pS_L | \bar{\psi}(0) \mathcal{U}[0, r]$$

$$\times \frac{\gamma^+ \gamma^5}{2} \psi(r) | pS_L \rangle_{r^+ = 0}. \tag{2}$$

---

[1]We thank Raju Venugopalan for pointing out this interpretation.

Note that antisymmetrization over the target proton spin projection on the beam axis $S_L = \pm 1$ is "optional"; parity symmetry guarantees that antisymmetry in the quark spin is sufficient, so that we may equivalently just set $S_L = +1$. Our convention for light-cone coordinates is $v^{\pm} = (v^0 \pm v^3)/\sqrt{2}$ and the proton is moving in the light-cone "plus" direction.

Our first goal is to simplify Eq. (2) at small x. The particulars of the Dirac structure in this forthcoming derivation will be specific to the helicity distribution because of the $\frac{1}{2}\gamma^{+}\gamma^5$ helicity projector in Eq. (2), but the overall approach will be common to any quark distribution at small x, such as transversity if we were to replace this matrix with the transversity projector $\frac{1}{2}\gamma^5\gamma^{+}\gamma^{\perp}$.

The formal definition (2) of the helicity TMD includes the process-dependent gauge link $\mathcal{U}[0, r]$; for SIDIS, the gauge link is explicitly given by

$$
\mathcal{U}[0, r] = \mathcal{P} \exp\left[ig \int_{+\infty}^{0} dz^- A^+(0^+, z^-, \underline{0}) \right]
$$
$$
\times \mathcal{P} \exp\left[-ig \int_{\underline{r}}^{\underline{0}} d\underline{z} \cdot \underline{A}(0^+, +\infty^-, \underline{z}) \right]
$$
$$
\times \mathcal{P} \exp\left[ig \int_{r^-}^{+\infty} dz^- A^+(0^+, z^-, \underline{r}) \right], \quad (3)
$$

where the gauge fields $A^\mu = A^{a\mu} t^a$ are color matrices and t^a are fundamental generators of SU(N_c). In the $A^- = 0$ gauge that we will employ here, one can neglect the transverse link at infinity, leaving just the lightlike, semi-infinite Wilson lines

$$
\mathcal{U}[0, r] = V_{\underline{0}}[0, \infty] V_{\underline{r}}[\infty, r^-], \quad (4)
$$

where we use the following notation for the fundamental Wilson lines,

$$
V_{\underline{x}}[b^-, a^-] = \mathcal{P} \exp\left[ig \int_{a^-}^{b^-} dx^- A^+(x^+ = 0, x^-, \underline{x}) \right]. \quad (5)
$$

Employing Eq. (4) in Eq. (2) we arrive at

$$
g_{1L}^q(x, k_T^2) = \frac{1}{(2\pi)^3} \int d^2r dr^-
$$
$$
\times e^{ik \cdot r} \langle p, S_L = +1 | \bar{\psi}(0) V_{\underline{0}}[0, \infty]
$$
$$
\times V_{\underline{r}}[\infty, r^-] \frac{\gamma^{+}\gamma^5}{2} \psi(r) | p, S_L = +1 \rangle_{r^+=0}. \quad (6)
$$

Inserting a complete set of states we get

$$
g_{1L}^q(x, k_T^2) = \frac{1}{(2\pi)^3} \sum_X \int d^2r dr^-
$$
$$
\times e^{ik \cdot r} \left(\frac{1}{2}\gamma^{+}\gamma^5 \right)_{\alpha\beta} \langle p, S_L = +1 | \bar{\psi}_\alpha(0) V_{\underline{0}}[0, \infty] | X \rangle
$$
$$
\times \langle X | V_{\underline{r}}[\infty, r^-] \psi_\beta(r) | p, S_L = +1 \rangle_{r^+=0}. \quad (7)
$$

Using this and converting to semiclassical operator averaging used in the saturation/color glass condensate (CGC) approach [45–52] (see [45,53–58] for reviews) gives

$$
g_{1L}^q(x, k_T^2) = \frac{2p^+}{(2\pi)^3} \sum_X \int d^2\zeta d\zeta^- d^2\xi d\xi^-
$$
$$
\times e^{ik \cdot (\zeta - \xi)} \left(\frac{1}{2}\gamma^{+}\gamma^5 \right)_{\alpha\beta} \langle \bar{\psi}_\alpha(\xi) V_{\underline{\xi}}[\xi^-, \infty] | X \rangle
$$
$$
\times \langle X | V_{\underline{\zeta}}[\infty, \zeta^-] \psi_\beta(\zeta) \rangle, \quad (8)
$$

where the angle brackets denote averaging in the target shock wave [25,26] where the target polarization $S_L = +1$ is implied, but not shown.

Identifying the Wilson lines with the quark propagating to the final state, one can think of Eq. (8) as containing the inclusive quark production amplitude squared. Hence we are back to the case of SIDIS considered in [59]. Equation (8) is represented graphically in Fig. 1. There, the shaded rectangles represent the target shock wave. The thin vertical line is the final state cut. The thick horizontal lines represent the Wilson lines, which are located at different transverse plane positions $\underline{\zeta}$ and $\underline{\xi}$ on either side of the cut. The diagrams in Fig. 1 are classified according to whether each of ζ^- and ξ^- are negative, positive, or zero (corresponding to the quark field being inside the shock wave). Diagrams in the B category also include the $\zeta^- > 0, \xi^- < 0$ contribution, which is not shown explicitly in Fig. 1. Similarly, diagrams E also include $\zeta^- < 0, \xi^- = 0$ contribution, while F graphs also include $\zeta^- > 0, \xi^- = 0$ ordering: while neither of those are shown in Fig. 1, it is implied that they have to be included.

Diagram A, evaluated at the lowest quasiclassical order with quarks exchanged in the t-channel interaction with the target, is the handbag diagram. Diagram B, along with the $\zeta^- > 0, \xi^- < 0$ contribution, is the 1-loop answer found in [59]. Diagram D does not allow for a spin-dependent interaction with the target, since both the ζ and ξ vertices are located after the shock wave. Hence, diagram D does not contribute. Diagrams C, E, and F have to be investigated separately, along with diagram A.

A more detailed representation of the types of diagrams that may contribute up to and including order α_s is given in Fig. 2. (In our power counting the interactions with the shock wave are considered to be of order one.) For each diagram class we show only one sample correction: for
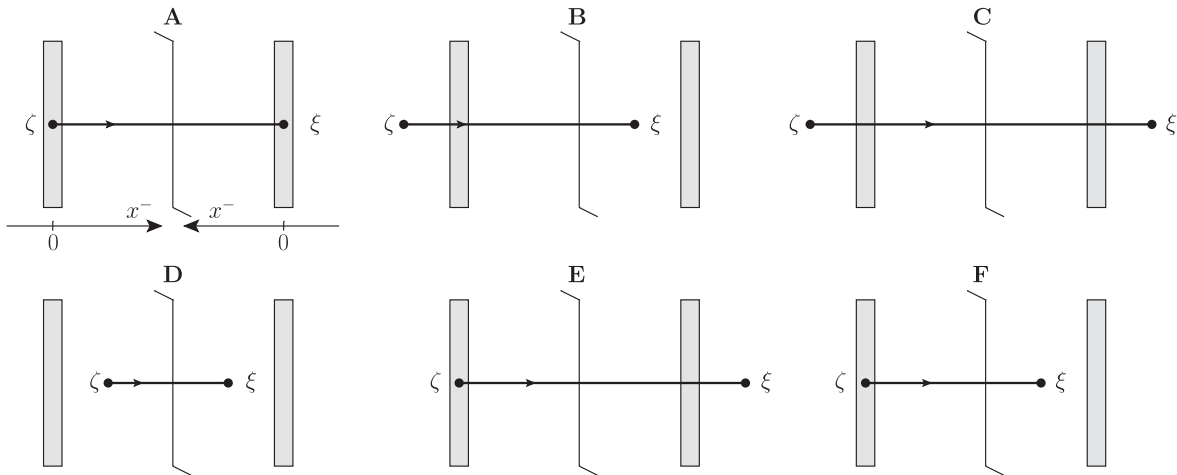
FIG. 1.   The main types of diagrams contributing to the quark helicity TMD in Eq. (8).

instance, in diagram A the gluon can also be both emitted and absorbed in the amplitude or in the complex conjugate amplitude, in diagram C the t-channel exchanges can take place on either side of the cut, while in diagram E the gluon can be emitted from the Wilson line on either side of the cut. The box in diagram B represents spin-dependent subeikonal interaction with the target, following the convention introduced in [9]. (The interaction will be detailed below, but it includes the t-channel quark exchanges with the target shown in other graphs.) We will be working in $A^- = 0$ light-cone gauge throughout this paper.

Diagram C appears to contribute; however, the interactions of the quark like with the target cancel if we move the t-channel exchanges across the cut [59]. Hence diagram C does not contribute at this order. (At the order α_s^2 diagram C can contribute; this is the order beyond the one considered explicitly here. Still we believe that the

leading-logarithmic contribution of diagram C will be canceled even at that order in the coupling due to the same mechanism as described in Appendix A.) Diagram F is energy suppressed, since the gluon in it has to be emitted and absorbed over a very short lifetime of the shock wave in the x^- direction. (Moreover, at small x the gluon in diagram F has to carry the same large "minus" momentum as the s-channel antiquark propagator connecting to the vertex ξ; the merger of this gluon with the Wilson line that begins at ζ cannot be eikonal, since the gluon and the quark propagator that this Wilson line represents carry comparable "minus" momenta.) Diagram E may contribute (as we have mentioned, the gluon there may connect to either one of the Wilson lines to the left and right of the cut). Diagram A may be "dressed" by gluon interactions with the Wilson lines, as shown in Fig. 2. In Appendix A we show that diagrams A and E cancel at the order α_s
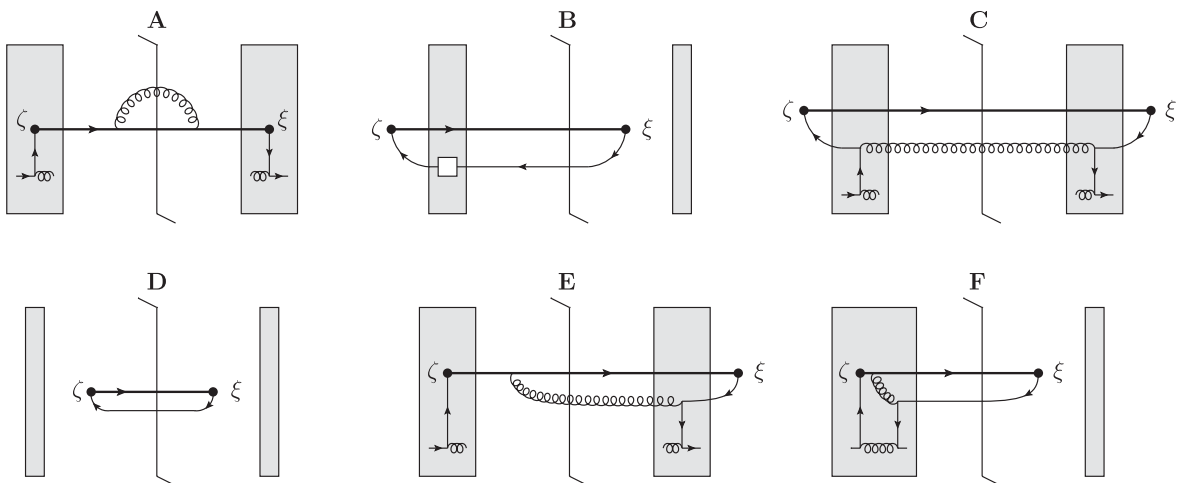
FIG. 2.   Diagrams contributing to the quark TMD defined in Eq. (8) with the order-α_s corrections due to s-channel gluon emissions shown explicitly. The thinner solid lines denote quark propagators, while the thicker solid lines are the Wilson lines (as in Fig. 1).

considered in Fig. 2 (and in the leading logarithmic approximation in x) and discuss what happens at higher orders in the coupling.[2]

We conclude that diagrams A and C–F do not contribute at the leading small-x level. Therefore, we are left with diagram B and its "mirror image," the contribution with $\zeta^- > 0, \xi^- < 0$. The mirror image is just complex conjugate of diagram B. Hence, diagram B and its mirror image give

$$
g_{1L}^q(x, k_T^2) = \frac{2p^+}{(2\pi)^3} \sum_{\bar{q}} \int_{-\infty}^0 d\zeta^- \int_0^\infty d\xi^- \int d^2\zeta d^2\xi \, e^{ik\cdot(\zeta-\xi)}
$$

$$
\times \left(\frac{1}{2}\gamma^+\gamma^5\right)_{\alpha\beta} \langle \bar{\psi}_\alpha(\xi) V_{\underline{\xi}}[\xi^-, \infty] | \bar{q} \rangle
$$

$$
\times \langle \bar{q} | V_{\underline{\zeta}}[\infty, \zeta^-] \psi_\beta(\zeta) \rangle + \text{c.c.}, \tag{9}
$$

where we have replaced $X \to \bar{q}$ since only the antiquark is produced in the final state (in addition to the quark represented by the Wilson lines). The sum $\sum_{\bar{q}}$ now denotes the Lorentz-invariant integral over the antiquark momentum and a sum over its polarizations and colors. Putting $V_{\underline{\xi}}[\xi^-, \infty] = 1$ for $\xi^- > 0$ (since the Wilson line does not cross the shock wave, it is trivial) and replacing $V_{\underline{\zeta}}[\infty, \zeta^-] \to V_{\underline{\zeta}}[\infty, -\infty]$ for $\zeta^- < 0$ since this Wilson
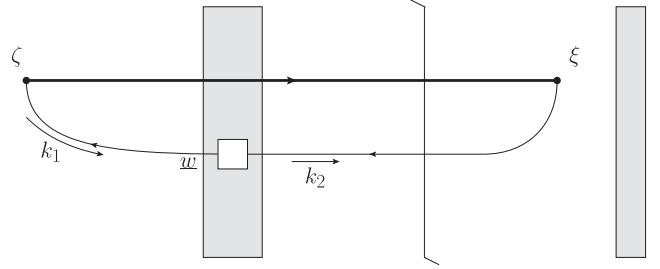
FIG. 3. A more detailed illustration of diagram B.

line crosses the shock wave and gets all the nontrivial contributions from this crossing only, we simplify (9) to

$$
g_{1L}^q(x, k_T^2) = \frac{2p^+}{(2\pi)^3} \sum_{\bar{q}} \int_{-\infty}^0 d\zeta^- \int_0^\infty d\xi^- \int d^2\zeta d^2\xi \, e^{ik\cdot(\zeta-\xi)}
$$

$$
\times \left(\frac{1}{2}\gamma^+\gamma^5\right)_{\alpha\beta} \langle \bar{\psi}_\alpha(\xi) | \bar{q} \rangle \langle \bar{q} | V_{\underline{\zeta}}[\infty, -\infty] \psi_\beta(\zeta) \rangle
$$

$$
+ \text{c.c.} \tag{10}
$$

Diagram B is illustrated in a little more detail in Fig. 3.

In evaluating diagram B we impose the $\zeta^- < 0, \xi^- > 0$ ordering, which makes sure that the vertices at ζ and ξ are outside the shock wave. For the antiquark (background-field [25,26]) propagator in Fig. 3 traversing the shock wave we write

$$
\overline{\psi_\alpha^i(\xi)} \, \psi_\beta^j(\zeta) = \int d^2w \, \frac{d^4k_1}{(2\pi)^4} \frac{d^4k_2}{(2\pi)^4} \, e^{ik_1^+\zeta^-} \, e^{i\underline{k}_1\cdot(\underline{w}-\underline{\zeta})} \, e^{-ik_2^+\xi^-} \, e^{i\underline{k}_2\cdot(\underline{\xi}-\underline{w})}
$$

$$
\times \left\{ \left[\frac{-i\slashed{k}_1}{k_1^2 + i\epsilon}\right] \left[\left(\hat{V}_{\underline{w}}^\dagger\right)^{ji} (2\pi)\delta(k_1^- - k_2^-)\right] \left[-\slashed{k}_2 (2\pi)\delta(k_2^2)\right] \right\}_{\beta\alpha}, \tag{11}
$$

where i and j are the quark color indices. This quantity is constructed as an antiquark propagator: created by $\hat{d}^\dagger$ in $\psi_\beta(\zeta)$ and propagating with positive energy k_1^- through the shockwave to be annihilated by $\hat{d}$ in $\bar{\psi}_\alpha(\xi)$. Note that the "vertex" for the antiquark passing through the shockwave (the box in Fig. 3) is a Dirac matrix, denoted by $(\hat{V}^\dagger)$. Its exact structure will be clarified later, but for now, in our small-x approximation, we can think of it as a light-cone Wilson line with or without an insertion of a noneikonal local operator.

In order to simplify the propagator (11) we first integrate over k_2^-, and over k_1^+ with k_2^+, while keeping in mind that $\zeta^- < 0$ and $\xi^- > 0$.[3] This yields

$$
\overline{\psi_\alpha^i(\xi)} \, \psi_\beta^j(\zeta) = \int d^2w \, \frac{d^2k_1 \, dk_1^-}{(2\pi)^3} \frac{d^2k_2}{(2\pi)^2} \, e^{i\frac{k_1^2}{2k_1^-}\zeta^- - i\frac{k_2^2}{2k_1^-}\xi^- + i\underline{k}_1\cdot(\underline{w}-\underline{\zeta}) + i\underline{k}_2\cdot(\underline{\xi}-\underline{w})} \, \theta(k_1^-)
$$

$$
\times \left\{ \left[\frac{\slashed{k}_1}{2k_1^-}\right] \left[\left(\hat{V}_{\underline{w}}^\dagger\right)^{ji}\right] \left[\frac{\slashed{k}_2}{2k_1^-}\right] \right\}_{\beta\alpha} \Bigg|_{k_2^- = k_1^-, k_1^2 = 0, k_2^2 = 0}. \tag{12}
$$

---

[2]Unlike the other diagrams considered here, diagram A does appear to contribute at order-1, that is, at Born level, when no gluon emission corrections like those shown in Fig. 2 are included. However, such contribution is independent of x, and is subleading compared to the contribution of diagram B we calculate below, which grows as a power of $1/x$.

[3]Here and below in this paper, when calculating diagrams like B, we will neglect the nonlogarithmic instantaneous terms; in this case the instantaneous term leads to the delta function $\delta(\zeta^-)$ confining the corresponding vertex to the inside of the shockwave. Such terms contribute to diagrams A, E, and F only. This means that in Eq. (11) one should understand $\slashed{k}_1$ as $\gamma^- \frac{k_1^2}{2k_1^-} + \gamma^+ k_1^- - \underline{\gamma}\cdot\underline{k}_1$.

Plugging this back into Eq. (10) and integrating over $\underline{\xi}$ and $\underline{k}_2$ we obtain

$$g^q_{1L}(x, k^2_T) = \frac{2p^+}{(2\pi)^3} \int_{-\infty}^0 d\zeta^- \int_0^\infty d\xi^- \int d^2\zeta e^{ik^+(\zeta^- - \xi^-)} \left(\frac{1}{2}\gamma^+\gamma^5\right)_{\alpha\beta} \left\langle TV^{ij}_{\underline{\zeta}}[\infty, -\infty] \int d^2w \frac{d^2k_1 dk_1^-}{(2\pi)^3} \right.$$

$$\left. \times e^{i\frac{k_1^2}{2k_1^-}\zeta^- - i\frac{k^2}{2k_1^-}\xi^- + i(\underline{k}_1 + \underline{k})\cdot(\underline{w} - \underline{\zeta})} \theta(k_1^-) \left\{ \left[\frac{\slashed{k}_1}{2k_1^-}\right] [(\hat{V}^\dagger_{\underline{w}})^{ji}] \left[\frac{\slashed{k}_2}{2k_1^-}\right] \right\}_{\beta\alpha} \right\rangle \Bigg|_{k_2^- = k_1^-, k_1^2 = 0, k_2^2 = 0, \underline{k}_2 = -\underline{k}} + \text{c.c.} \quad (13)$$

Here we explicitly insert the time-ordering sign T, which is often omitted but implied in the CGC calculations. Since both "Wilson lines" $V_{\underline{\zeta}}$ and $\hat{V}_{\underline{w}}$ are in the amplitude of diagram B in Fig. 3, they come in with a time-ordering sign. Distinguishing time-ordered and antitime ordered correlation functions will be very important below. As we detail in Appendix B, inserting time-ordering sign T and the antitime ordering sign $\bar{T}$ allow us to distinguish amplitudes from the complex conjugate amplitudes. This way we are able to differentiate between an expectation value of the complex conjugate operator in the amplitude versus the complex conjugate of the expectation value of the operator in the amplitude.

Next we integrate over ζ^- and ξ^-. This yields

$$g^q_{1L}(x, k^2_T) = -\frac{2p^+}{(2\pi)^3} \int d^2\zeta d^2w \frac{d^2k_1 dk_1^-}{(2\pi)^3} e^{i(\underline{k}_1 + \underline{k})\cdot(\underline{w} - \underline{\zeta})} \theta(k_1^-) \left\langle TV^{ij}_{\underline{\zeta}}[\infty, -\infty] \text{Tr}\left[\frac{1}{2}\gamma^+\gamma^5 \slashed{k}_1 (\hat{V}^\dagger_{\underline{w}})^{ji} \slashed{k}_2\right] \right\rangle$$

$$\times \frac{1}{[2k_1^- k^+ + \underline{k}_1^2 - i\epsilon k_1^-][2k_1^- k^+ + \underline{k}^2 + i\epsilon k_1^-]} \Bigg|_{k_2^- = k_1^-, k_1^2 = 0, k_2^2 = 0, \underline{k}_2 = -\underline{k}} + \text{c.c.} \quad (14)$$

Introducing polarization sums, we write

$$g^q_{1L}(x, k^2_T) = -\frac{2p^+}{(2\pi)^3} \int d^2\zeta d^2w \frac{d^2k_1 dk_1^-}{(2\pi)^3} e^{i(\underline{k}_1 + \underline{k})\cdot(\underline{w} - \underline{\zeta})} \theta(k_1^-) \sum_{\sigma_1, \sigma_2} \bar{v}_{\sigma_2}(k_2) \frac{1}{2}\gamma^+\gamma^5 v_{\sigma_1}(k_1) \langle TV^{ij}_{\underline{\zeta}}[\infty, -\infty]$$

$$\times \bar{v}_{\sigma_1}(k_1)(\hat{V}^\dagger_{\underline{w}})^{ji} v_{\sigma_2}(k_2) \rangle \frac{1}{[2k_1^- k^+ + \underline{k}_1^2 - i\epsilon k_1^-][2k_1^- k^+ + \underline{k}^2 + i\epsilon k_1^-]} \Bigg|_{k_2^- = k_1^-, k_1^2 = 0, k_2^2 = 0, \underline{k}_2 = -\underline{k}} + \text{c.c.} \quad (15)$$

Further, we define the (antiquark) polarized "Wilson line" as a longitudinal spin-dependent part of an antiquark scattering amplitude on the shock wave. We need the part of the scattering amplitude proportional to the Pauli matrix σ^3 in helicity space, that is, to $\sigma\delta_{\sigma\sigma'}$ with σ and σ' the helicities of the antiquark before and after scattering respectively. Using the Brodsky-Lepage (BL) spinors [60] we write

$$[\bar{v}_\sigma(p)(\hat{V}^\dagger_{\underline{x}}) v_{\sigma'}(p')] = 2\sqrt{p^- p'^-} \delta_{\sigma\sigma'}(V^\dagger_{\underline{x}} - \sigma V^{\text{pol}\dagger}_{\underline{x}} + \cdots) = 2\sqrt{p^- p'^-} \delta_{\sigma\sigma'} V^\dagger_{\underline{x}}(-\sigma) + \cdots, \quad (16)$$

where the ellipsis denote the subeikonal corrections independent of helicity, which we are not interested in and we use a shorthand notation $V_{\underline{x}} \equiv V_{\underline{x}}[\infty, -\infty]$.[4]

In addition, we will employ

$$\bar{v}_{\sigma_2}(k_2) \frac{1}{2}\gamma^+\gamma^5 v_{\sigma_1}(k_1) = \frac{1}{2}\sigma_2\delta_{\sigma_2\sigma_1} \frac{(\underline{k}_2 \cdot \underline{k}_1) - i\sigma_2(\underline{k}_2 \times \underline{k}_1)}{\sqrt{k_1^- k_2^-}} \quad (18)$$

for the ($\pm$)-interchanged Brodsky-Lepage spinors (which we will also refer to as the anti-BL spinors).

---

[4]The general convention for BL spinors is as follows (these matrix elements appear either in the scattering amplitude or in the complex conjugate amplitude):

$$\bar{u}_\sigma(p)(\hat{V}_{\underline{x}}) u_{\sigma'}(p') = 2\sqrt{p^- p'^-} \delta_{\sigma\sigma'} V_{\underline{x}}(\sigma), \qquad \bar{u}_\sigma(p)(\hat{V}^\dagger_{\underline{x}}) u_{\sigma'}(p') = 2\sqrt{p^- p'^-} \delta_{\sigma\sigma'} V^\dagger_{\underline{x}}(\sigma), \quad (17a)$$

$$\bar{v}_\sigma(p)(\hat{V}_{\underline{x}}) v_{\sigma'}(p') = 2\sqrt{p^- p'^-} \delta_{\sigma\sigma'} V_{\underline{x}}(-\sigma), \qquad \bar{v}_\sigma(p)(\hat{V}^\dagger_{\underline{x}}) v_{\sigma'}(p') = 2\sqrt{p^- p'^-} \delta_{\sigma\sigma'} V^\dagger_{\underline{x}}(-\sigma). \quad (17b)$$

Using the matrix elements from Eqs. (16) and (18) in Eq. (15) we obtain

$$g_{1L}^q(x,k_T^2) = \frac{2p^+}{(2\pi)^3} \int d^2\zeta d^2w \frac{d^2k_1 dk_1^-}{(2\pi)^3} e^{i(\underline{k}_1+\underline{k})\cdot(\underline{w}-\underline{\zeta})} \theta(k_1^-) \sum_{\sigma_1} \sigma_1 [\underline{k}\cdot\underline{k}_1 - i\sigma_1 \underline{k}\times\underline{k}_1]$$

$$\times \langle \mathrm{Ttr}[V_{\underline{\zeta}}^{ij}[\infty,-\infty]V_{\underline{w}}^\dagger(-\sigma_1)]\rangle \frac{1}{[2k_1^-k^+ + \underline{k}_1^2 - i\epsilon k_1^-][2k_1^-k^+ + \underline{k}^2 + i\epsilon k_1^-]} + \mathrm{c.c.} \qquad (19)$$

Remembering that $k^+ = xp^+$ and we are considering the small-x regime (and, hence, $2k_1^- k^+ = 2k_1^- x p^+ \ll \underline{k}^2, \underline{k}_1^2$), we get

$$g_{1L}^q(x,k_T^2) = \frac{2p^+}{(2\pi)^3} \int d^2\zeta d^2w \frac{d^2k_1 dk_1^-}{(2\pi)^3} e^{i(\underline{k}_1+\underline{k})\cdot(\underline{w}-\underline{\zeta})} \theta(k_1^-) \sum_{\sigma_1} \sigma_1 \frac{\underline{k}\cdot\underline{k}_1 - i\sigma_1 \underline{k}\times\underline{k}_1}{\underline{k}_1^2 \underline{k}^2} \langle \mathrm{Ttr}[V_{\underline{\zeta}}V_{\underline{w}}^\dagger(-\sigma_1)]\rangle + \mathrm{c.c.} \quad (20)$$

Writing $V_{\underline{w}}^\dagger(-\sigma_1) = V_{\underline{w}}^\dagger - \sigma_1 V_{\underline{w}}^{\mathrm{pol}\dagger}$ allows us to sum over σ_1 obtaining, after performing $\underline{k}_1$ integration as well,

$$g_{1L}^q(x,k_T^2) = \frac{4p^+ i}{(2\pi)^4} \int d^2\zeta d^2w \, e^{-i\underline{k}\cdot(\underline{\zeta}-\underline{w})} \int_0^\infty \frac{dk_1^-}{2\pi} \left\{ \frac{\underline{k}}{\underline{k}^2}\cdot\frac{\underline{\zeta}-\underline{w}}{|\underline{\zeta}-\underline{w}|^2} \langle \mathrm{Ttr}[V_{\underline{\zeta}}V_{\underline{w}}^{\mathrm{pol}\dagger}] + \bar{\mathrm{T}}\mathrm{tr}[V_{\underline{\zeta}}^{\mathrm{pol}}V_{\underline{w}}^\dagger]\rangle + i\frac{\underline{k}}{\underline{k}^2}\times\frac{\underline{\zeta}-\underline{w}}{|\underline{\zeta}-\underline{w}|^2} \langle \mathrm{Ttr}[V_{\underline{\zeta}}V_{\underline{w}}^\dagger] \right.$$

$$\left. - \bar{\mathrm{T}}\mathrm{tr}[V_{\underline{\zeta}}V_{\underline{w}}^\dagger]\rangle \right\}, \qquad (21)$$

where we have explicitly added the complex conjugate term (and interchanged $\underline{\zeta} \leftrightarrow \underline{w}$ in it) by employing the fact that $[\mathrm{T}O_1(x)O_2(y)]^\dagger = \bar{\mathrm{T}}O_2^\dagger(y)O_1^\dagger(x)$ for two operators $O_1(x)$ and $O_2(y)$. As mentioned before, the sign $\bar{\mathrm{T}}$ denotes antitime ordering.

Before we continue, let us stress the importance of the ordering of (polarized and/or unpolarized) Wilson lines in the nontime-ordered correlation functions. To do this, let us introduce the following useful relations between the expectation values of Wilson lines:

$$\langle \mathrm{Ttr}[V_{\underline{x}}V_{\underline{y}}^{\mathrm{pol}\dagger}]\rangle = \langle \mathrm{tr}[V_{\underline{x}}V_{\underline{y}}^{\mathrm{pol}\dagger}]\rangle, \qquad (22a)$$

$$\langle \bar{\mathrm{T}}\mathrm{tr}[V_{\underline{x}}V_{\underline{y}}^{\mathrm{pol}\dagger}]\rangle = \langle \mathrm{tr}[V_{\underline{y}}^{\mathrm{pol}\dagger}V_{\underline{x}}]\rangle. \qquad (22b)$$

The relations Eqs. (22) are written here for one regular Wilson line and for one unpolarized Wilson line; however, they are also valid for correlators of two regular Wilson lines. The order of the Wilson lines under the trace matters for the right-hand sides of Eqs. (22). In the sense of Eq. (8), the right Wilson line in each nontime-ordered correlator can be thought of as contributing to the amplitude, while the left Wilson line contributes to the complex conjugate amplitude. The Wilson lines are bosonic operators (even the polarized Wilson lines are bosonic, as we will see below); hence the ordering of the Wilson lines is not important for the (anti)time-ordered correlation functions.

Note that this ordering issue does not apply to the standard eikonal CGC calculations done in the leading-logarithmic approximation (LLA) [25–32], where all the Wilson lines are standard eikonal Wilson lines, and the background gluon field is assumed to be classical [47–52]

rather than being an operator; in such case the order of Wilson lines does not matter and Eqs. (22) are trivially satisfied (see [61] for applications of that result to inclusive gluon production). The relations (22) were shown to work in [62] up to next-to-leading logarithms (NLL) in x for the unpolarized BK/JIMWLK evolution.

Diagrammatically the relations (22) can be pictured as arising from the reflection symmetry of light-cone Wilson lines (true "unpolarized" Wilson lines) with respect to the final state cut. Equation (22a) can be thought of as being due to reflecting a light-cone Wilson line from the complex conjugate amplitude (on the expression's right-hand side) back into the amplitude [the left-hand side of Eq. (22b)], as illustrated in Fig. 4. Equation (22b) arises after the reflection of the light-cone Wilson line from the amplitude into the complex conjugate amplitude.

Taking the real and imaginary parts of Eqs. (22) one obtains more useful formulas

$$2\mathrm{Re}\langle \mathrm{Ttr}[V_{\underline{x}}V_{\underline{y}}^{\mathrm{pol}\dagger}]\rangle = \langle \mathrm{tr}[V_{\underline{x}}V_{\underline{y}}^{\mathrm{pol}\dagger}]\rangle + \langle \mathrm{tr}[V_{\underline{y}}^{\mathrm{pol}}V_{\underline{x}}^\dagger]\rangle, \qquad (23a)$$

$$2i\mathrm{Im}\langle \mathrm{Ttr}[V_{\underline{x}}V_{\underline{y}}^{\mathrm{pol}\dagger}]\rangle = \langle \mathrm{tr}[V_{\underline{x}}V_{\underline{y}}^{\mathrm{pol}\dagger}]\rangle - \langle \mathrm{tr}[V_{\underline{y}}^{\mathrm{pol}}V_{\underline{x}}^\dagger]\rangle, \qquad (23b)$$
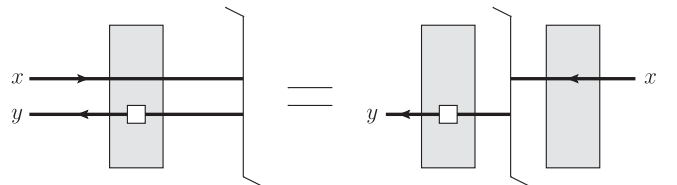
FIG. 4. The reflection of the Wilson line from the complex conjugate amplitude to the amplitude discussed in the text.

$$2\text{Re}\langle \bar{\text{T}}\text{tr}[V_{\underline{x}}V_{\underline{y}}^{\text{pol}\dagger}]\rangle = \langle\text{tr}[V_{\underline{y}}^{\text{pol}\dagger}V_{\underline{x}}]\rangle + \langle\text{tr}[V_{\underline{x}}^{\dagger}V_{\underline{y}}^{\text{pol}}]\rangle, \quad (23c)$$

$$2i\text{Im}\langle \bar{\text{T}}\text{tr}[V_{\underline{x}}V_{\underline{y}}^{\text{pol}\dagger}]\rangle = \langle\text{tr}[V_{\underline{y}}^{\text{pol}\dagger}V_{\underline{x}}]\rangle - \langle\text{tr}[V_{\underline{x}}^{\dagger}V_{\underline{y}}^{\text{pol}}]\rangle. \quad (23d)$$

Returning to Eq. (21) we notice that

$$\langle\bar{\text{T}}\text{tr}[V_{\underline{\zeta}}V_{\underline{w}}^{\dagger}] - \bar{\text{T}}\text{tr}[V_{\underline{\zeta}}V_{\underline{w}}^{\dagger}]\rangle = \langle\text{tr}[V_{\underline{\zeta}}V_{\underline{w}}^{\dagger}] - \text{tr}[V_{\underline{w}}^{\dagger}V_{\underline{\zeta}}]\rangle = 0,$$
$$(24)$$

since for true Wilson lines the reflection symmetries that led to Eqs. (21) also imply that $\langle\text{tr}[V_{\underline{\zeta}}V_{\underline{w}}^{\dagger}]\rangle = \langle\text{tr}[V_{\underline{w}}^{\dagger}V_{\underline{\zeta}}]\rangle$ [with the same NLL accuracy as Eqs. (22) were verified up to]. (Note that $\bar{\text{T}}\text{tr}[V_{\underline{\zeta}}V_{\underline{w}}^{\dagger}] - \bar{\text{T}}\text{tr}[V_{\underline{\zeta}}V_{\underline{w}}^{\dagger}]$ is not the odderon operator. The latter is $\text{tr}[V_{\underline{\zeta}}V_{\underline{w}}^{\dagger}] - \text{tr}[V_{\underline{w}}V_{\underline{\zeta}}^{\dagger}]$ [63,64] and it gives zero after the impact parameter integration, as observed in [65].)

Since the second term in the curly brackets of Eq. (21) is zero, we arrive at

$$g_{1L}^{q}(x, k_T^2) = \frac{4p^+i}{(2\pi)^4}\int d^2\zeta d^2w e^{-i\underline{k}\cdot(\underline{\zeta}-\underline{w})}\int_0^\infty \frac{dk_1^-}{2\pi}\frac{\underline{k}}{\underline{k}^2}\cdot\frac{\underline{\zeta}-\underline{w}}{|\underline{\zeta}-\underline{w}|^2}\langle\bar{\text{T}}\text{tr}[V_{\underline{\zeta}}V_{\underline{w}}^{\text{pol}\dagger}] + \bar{\text{T}}\text{tr}[V_{\underline{\zeta}}^{\text{pol}}V_{\underline{w}}^{\dagger}]\rangle. \quad (25)$$

In the flavor-singlet case that we are primarily interested in here one adds the antiquark TMD contribution. This yields

$$g_{1L}^{S}(x, k_T^2) = \frac{4p^+i}{(2\pi)^4}\int d^2\zeta d^2w e^{-i\underline{k}\cdot(\underline{\zeta}-\underline{w})}\int_0^\infty \frac{dk_1^-}{2\pi}\frac{\underline{k}}{\underline{k}^2}\cdot\frac{\underline{\zeta}-\underline{w}}{|\underline{\zeta}-\underline{w}|^2}$$
$$\times \langle\bar{\text{T}}\text{tr}[V_{\underline{\zeta}}V_{\underline{w}}^{\text{pol}\dagger}] + \bar{\text{T}}\text{tr}[V_{\underline{w}}^{\text{pol}}V_{\underline{\zeta}}^{\dagger}] + \bar{\text{T}}\text{tr}[V_{\underline{\zeta}}^{\text{pol}}V_{\underline{w}}^{\dagger}] + \bar{\text{T}}\text{tr}[V_{\underline{w}}V_{\underline{\zeta}}^{\text{pol}\dagger}]\rangle. \quad (26)$$

Here we have used (again for the anti-BL spinors)

$$\bar{u}_{\sigma_2}(k_2)\frac{1}{2}\gamma^+\gamma^5 u_{\sigma_1}(k_1) = -\frac{1}{2}\sigma_2\delta_{\sigma_2\sigma_1}\frac{(\underline{k}_2\cdot\underline{k}_1) + i\sigma_2(\underline{k}_2\times\underline{k}_1)}{\sqrt{k_1^-k_2^-}}. \quad (27)$$

We next define the (flavor-singlet) polarized dipole amplitude

$$G_{\underline{w},\underline{\zeta}}(zs) = \frac{k_1^-p^+}{N_c}\text{Re}\langle\bar{\text{T}}\text{tr}[V_{\underline{\zeta}}V_{\underline{w}}^{\text{pol}\dagger}] + \bar{\text{T}}\text{tr}[V_{\underline{w}}^{\text{pol}}V_{\underline{\zeta}}^{\dagger}]\rangle \quad (28)$$

with $zs = 2k_1^-p^+$. This definition is different from the one used in our previous works [9–13] by the real-part operator Re and by the time-ordering signs shown explicitly here while they were only implied in our earlier works, as is customary in the saturation/CGC calculations (with the exception of [62]). All the calculations performed in [9–13] were not affected by the omitted time-ordering signs, since they were *de facto* applied. Similarly, the Re sign was *de facto* applied as well, since only cut diagrams were calculated. In DLA, the real-part operator only makes a difference when evaluating the initial conditions for the (linear) small-x evolution of the polarized dipole amplitude (28). In calculating these initial conditions the Re operator

from the right of Eq. (28) was applied: we calculated the scattering cross sections for the Born-level processes, instead of the whole forward amplitude. (That is, we calculated the imaginary part of the forward scattering amplitude.) In Appendix B we show explicitly how the calculations carried out earlier in Sec. II A of [11] are equivalent to Eq. (28), thus also illustrating how Eqs. (22) work.

Employing the definition (28) in Eq. (26) along with Eqs. (22) and their complex conjugates [or, equivalently, Eqs. (23) and their complex conjugates] while noticing that for a longitudinally polarized target, due to the absence of any preferred transverse direction,

$$\int d^2\left(\frac{\underline{\zeta}+\underline{w}}{2}\right)\langle\bar{\text{T}}\text{tr}[V_{\underline{\zeta}}V_{\underline{w}}^{\dagger}]\rangle \equiv h(|\underline{\zeta}-\underline{w}|) = h(|\underline{w}-\underline{\zeta}|) = \int d^2\left(\frac{\underline{\zeta}+\underline{w}}{2}\right)\langle\bar{\text{T}}\text{tr}[V_{\underline{w}}V_{\underline{\zeta}}^{\dagger}]\rangle \quad (29)$$

for correlators made out of both polarized and unpolarized Wilson lines with time-ordering and antitime ordering, we arrive at

$$g_{1L}^{S}(x, k_T^2) = \frac{8N_c i}{(2\pi)^5}\int d^2\zeta d^2w e^{-i\underline{k}\cdot(\underline{\zeta}-\underline{w})}\int_{\Lambda^2/s}^1 \frac{dz}{z}\frac{\underline{\zeta}-\underline{w}}{|\underline{\zeta}-\underline{w}|^2}\cdot\frac{\underline{k}}{\underline{k}^2}G_{\underline{w},\underline{\zeta}}(zs). \quad (30)$$

Here $s \approx Q^2/x$ is the center-of-mass energy squared, while Λ is an infrared (IR) cutoff with Λ^2/s the lowest possible value of the variable z. Introducing a dummy transverse vector variable $\underline{y}$ we rewrite Eq. (30) as

$$g_{1L}^S(x, k_T^2) = \frac{8N_c}{(2\pi)^6} \int d^2\zeta d^2w d^2y e^{-i\underline{k}\cdot(\underline{\zeta}-\underline{y})} \int_{\Lambda^2/s}^1 \frac{dz}{z} \frac{\underline{\zeta} - \underline{w}}{|\underline{\zeta} - \underline{w}|^2} \cdot \frac{\underline{y} - \underline{w}}{|\underline{y} - \underline{w}|^2} G_{\underline{w},\underline{\zeta}}(zs), \tag{31}$$

in complete agreement with Eq. (8c) in [11], or, equivalently, Eq. (15) in [9].

The corresponding flavor-singlet quark helicity PDF is given by [9–13]

$$\sum_f [\Delta q^f(x, Q^2) + \Delta\bar{q}^f(x, Q^2)] = \sum_f \int d^2k_T g_{1L}^S(x, k_T^2) = \frac{N_c N_f}{2\pi^3} \int_{\Lambda^2/s}^1 \frac{dz}{z} \int_{\frac{1}{zs}}^{\frac{1}{zQ^2}} \frac{dx_{10}^2}{x_{10}^2} G(x_{10}^2, z), \tag{32}$$

where

$$G(x_{10}^2, z) = \int d^2\left(\frac{\underline{x}_1 + \underline{x}_0}{2}\right) G_{10}(z) \tag{33}$$

with $G_{10} = G_{\underline{x}_1, \underline{x}_0}$ and $\underline{x}_{10} = \underline{x}_1 - \underline{x}_0$.

For the flavor nonsinglet distribution we have to *subtract* the antiquark contribution out of Eq. (25):

$$g_{1L}^{NS}(x, k_T^2) = \frac{4p^+ i}{(2\pi)^4} \int d^2\zeta d^2w e^{-i\underline{k}\cdot(\underline{\zeta}-\underline{w})} \int_0^\infty \frac{dk_1^-}{2\pi} \frac{\underline{k}}{k^2} \cdot \frac{\underline{\zeta} - \underline{w}}{|\underline{\zeta} - \underline{w}|^2}$$
$$\times \langle \text{Ttr}[V_{\underline{\zeta}} V_{\underline{w}}^{\text{pol}\dagger}] - \text{Ttr}[V_{\underline{w}}^{\text{pol}} V_{\underline{\zeta}}^\dagger] + \bar{\text{T}}\text{tr}[V_{\underline{\zeta}}^{\text{pol}} V_{\underline{w}}^\dagger] - \bar{\text{T}}\text{tr}[V_{\underline{w}} V_{\underline{\zeta}}^{\text{pol}\dagger}] \rangle. \tag{34}$$

Similarly, define the flavor non-singlet polarized dipole amplitude

$$G_{\underline{w},\underline{\zeta}}^{NS}(zs) = \frac{k_1^- p^+}{N_c} \text{Re} \langle \text{Ttr}[V_{\underline{\zeta}} V_{\underline{w}}^{\text{pol}\dagger}] - \text{Ttr}[V_{\underline{w}}^{\text{pol}} V_{\underline{\zeta}}^\dagger] \rangle = \frac{k_1^- p^+}{N_c} \text{Re} \langle \text{tr}[V_{\underline{\zeta}} V_{\underline{w}}^{\text{pol}\dagger}] - \text{tr}[V_{\underline{\zeta}}^\dagger V_{\underline{w}}^{\text{pol}}] \rangle, \tag{35}$$

where we have used Eq. (22) and the complex conjugate of Eq. (22b) to simplify the definition. Using Eq. (35) in Eq. (34) we arrive at

$$g_{1L}^{NS}(x, k_T^2) = \frac{8N_c}{(2\pi)^6} \int d^2\zeta d^2w d^2y e^{-i\underline{k}\cdot(\underline{\zeta}-\underline{y})} \int_{\Lambda^2/s}^1 \frac{dz}{z} \frac{\underline{\zeta} - \underline{w}}{|\underline{\zeta} - \underline{w}|^2} \cdot \frac{\underline{y} - \underline{w}}{|\underline{y} - \underline{w}|^2} G_{\underline{w},\underline{\zeta}}^{NS}(zs), \tag{36}$$

in agreement with Eq. (54c) in [11]. Once again, the apparent difference between the definition of the flavor nonsinglet distribution in Eq. (55a) of [11] and Eq. (35) is due to the real-part (Re) operator and the time-ordering signs which were implied in [11], though not shown explicitly. Only cut diagrams were calculated in [11] for the initial condition of the nonsinglet polarized dipole evolution. Another reason for this absence of the Re sign causing no difference in that particular case is that the expression under the Re sign was already real (see Appendix B for details).

B. Gluon helicity TMDs

For completeness, let us quote here the results of [13], where the dipole and Weizsäcker-Williams (WW) gluon helicity TMDs were calculated at small x, also starting with the full operator expression.

Define another dipolelike polarized operator

$$G_{10}^i(zs) \equiv \frac{1}{2N_c} \langle \text{tr}[V_{\underline{0}} (V_{\underline{1}}^{\text{pol}\dagger})_\perp^i] + \text{c.c.} \rangle(zs) \tag{37}$$

with a different polarized fundamental Wilson line

$$(V_{\underline{x}}^{\text{pol}})_\perp^i \equiv \int_{-\infty}^{+\infty} dx^- V_{\underline{x}}[+\infty, x^-](igP^+ A_\perp^i(x)) V_{\underline{x}}[x^-, -\infty]$$
$$= \frac{1}{2} \int_{-\infty}^{+\infty} dx^- V_{\underline{x}}[+\infty, x^-](ig\bar{A}_\perp^i(x)) V_{\underline{x}}[x^-, -\infty]. \tag{38}$$

Applying Eq. (22a) we can rewrite Eq. (37) as

$$G_{10}^i(zs) \equiv \frac{1}{2N_c} \langle \text{Ttr}[V_{\underline{0}} (V_{\underline{1}}^{\text{pol}\dagger})_\perp^i] + \text{c.c.} \rangle(zs), \tag{39}$$

which facilitates its diagrammatic evaluation performed in [13].

After the integration over all impact parameters, the new polarized dipole amplitude is a vector-valued function of $\underline{x}_{10}$ only, with no other transverse vector present. We thus write [13]

$$\int d^2b_{10} G^i_{10}(zs) = (x_{10})^i_\perp G_1(x^2_{10}, zs) + \epsilon^{ij}_T (x_{10})^j_\perp G_2(x^2_{10}, zs). \tag{40}$$

Employing these quantities we write the dipole gluon helicity TMD at small x as [13]

$$g^{Gdip}_{1L}(x, k^2_T) = \frac{-N_c}{\alpha_s 2\pi^4} \int d^2x_{10} e^{i\underline{k}\cdot\underline{x}_{10}} \left[1 + x^2_{10} \frac{\partial}{\partial x^2_{10}}\right] G_2\left(x^2_{10}, zs = \frac{Q^2}{x}\right). \tag{41}$$

The WW gluon helicity TMD is [13]

$$g^{GWW}_{1L}(x, k^2_T) = \frac{1}{\alpha_s\pi(2\pi)^3} \int d^2x_{10} d^2b_{10} e^{i\underline{k}\cdot\underline{x}_{10}} \epsilon^{ij}_T \left\langle \text{tr}\left[(V^{\text{pol}}_{\underline{1}})^i_\perp V^\dagger_{\underline{1}} V_{\underline{0}}\left(\frac{\partial}{\partial(x_0)^j_\perp} V^\dagger_{\underline{0}}\right)\right] + \text{c.c.}\right\rangle. \tag{42}$$

Finally, the gluon helicity PDF is given by

$$\Delta G(x, Q^2) = \int d^2k\, g^{GWW}_{1L}(x, k^2_T) = \int d^2k\, g^{Gdip}_{1L}(x, k^2_T) = \frac{-2N_c}{\alpha_s\pi^2}\left[\left(1 + x^2_{10}\frac{\partial}{\partial x^2_{10}}\right) G_2\left(x^2_{10}, zs = \frac{Q^2}{x}\right)\right]_{x^2_{10} = \frac{1}{Q^2}}. \tag{43}$$

III. POLARIZED "WILSON LINES": OPERATOR DEFINITIONS

A. Polarized fundamental Wilson line

Our next goal is to construct an explicit expression for the polarized Wilson line operator $V^{\text{pol}}_{\underline{x}}$ that we have employed above and in [9–13]. To find this operator we have to calculate the scattering amplitude of a high-energy longitudinally polarized quark on a longitudinally polarized target, keeping only the polarization-dependent part of the interaction with the background gluon and quark fields. There are two contributions in this calculation, as shown in the two panels of Fig. 5: polarized gluon (left panel) and quarks (right panel) exchanges. The gluon-exchange contribution in the left panel of Fig. 5 has already been calculated in [13]. Hence all that is left to do is to find the contribution of the quark exchanges from the right panel.

The expression for the polarized fundamental Wilson line with a single t-channel gluon exchange carrying the polarization information, corresponding to the left panel of Fig. 5, is given by Eq. (21) of [13]:

$$(V^{\text{pol}}_{\underline{x}})^g = \frac{igp^+_1}{s}\int^\infty_{-\infty} dx^- V_{\underline{x}}[+\infty, x^-] F^{12}(x^-, \underline{x}) V_{\underline{x}}[x^-, -\infty]. \tag{44}$$

Our aim now is to find $(V^{\text{pol}}_{\underline{x}})^q$. Let us repeat the calculation from Sec. II B of [13], but now including quark exchanges in the t-channel, as shown in the right panel of Fig. 5 (exactly what happens to the quark inside the target is not important for our calculation, as long as the target generates the quark fields ψ or $\bar\psi$). To do so, let us first calculate the contribution of the left t-channel quark exchange in the right panel of Fig. 5,

$$\frac{1}{2p^-_2} \epsilon^{\mu*}_\lambda(p_2 + k)(ig)\bar\psi(k)t^a\gamma_\mu u_\sigma(p_2)$$

$$= -\frac{ig}{\sqrt{\sqrt{2}p^-_2}}\bar\psi(k)t^a\rho(\sigma)\delta_{\sigma,\lambda}, \tag{45}$$

where we have defined the $+ \leftrightarrow -$ interchanged Brodsky-Lepage spinors $u_\sigma(p_2) = \sqrt{\sqrt{2}p^-_2}\rho(\sigma)$ for massless quarks with momentum $p^\mu_2 = (0, p^-_2, \underline{0})$ (cf. [60]). Here

$$\rho(+1) = \frac{1}{\sqrt{2}}\begin{pmatrix}1\\0\\-1\\0\end{pmatrix}, \qquad \rho(-1) = \frac{1}{\sqrt{2}}\begin{pmatrix}0\\1\\0\\1\end{pmatrix}, \tag{46}$$

FIG. 5. Two contributions to the polarized fundamental Wilson line in a background field. Filled circles at the quark-gluon vertices denote the spin-dependent subeikonal scattering.

and we neglected terms further suppressed by $1/p_2^-$. Fourier transforming (45) we get

$$-\frac{ig}{\sqrt{\sqrt{2}p_2^-}}\bar{\psi}(x_1^-,\underline{x})t^a\rho(\sigma)\delta_{\sigma,\lambda}. \qquad (47)$$

Similarly, the contribution of the right t-channel exchange of the right panel in Fig. 5 gives

$$-\frac{ig}{\sqrt{\sqrt{2}p_2^-}}\rho^T(\sigma')t^b\gamma^0\psi(x_2^-,\underline{x})\delta_{\sigma',\lambda}. \qquad (48)$$

Combining Eqs. (47) and (48) we write the operator, the $\sigma\delta_{\sigma\sigma'}$-dependent part of which would give us the polarized Wilson line:

$$\begin{aligned}
\sigma\delta_{\sigma\sigma'}(V_{\underline{x}}^{\text{pol}})^q \supset\ & -\frac{g^2 p_1^+\sqrt{2}}{s}\int_{-\infty}^{\infty}dx_1^-\int_{x_1^-}^{\infty}dx_2^-\sum_{\lambda}V_{\underline{x}}[+\infty,x_2^-]\rho^T(\sigma')t^b\gamma^0\psi(x_2^-,\underline{x})\delta_{\sigma',\lambda}U_{\underline{x}}^{ba}[x_2^-,x_1^-]\\
&\times\bar{\psi}(x_1^-,\underline{x})t^a\rho(\sigma)\delta_{\sigma,\lambda}V_{\underline{x}}[x_1^-,-\infty]\\
=\ & -\delta_{\sigma\sigma'}\frac{g^2 p_1^+\sqrt{2}}{s}\int_{-\infty}^{\infty}dx_1^-\int_{x_1^-}^{\infty}dx_2^-V_{\underline{x}}[+\infty,x_2^-]\rho^T(\sigma)t^b\gamma^0\psi(x_2^-,\underline{x})U_{\underline{x}}^{ba}[x_2^-,x_1^-]\\
&\times\bar{\psi}(x_1^-,\underline{x})t^a\rho(\sigma)V_{\underline{x}}[x_1^-,-\infty]\\
=\ & -\delta_{\sigma\sigma'}\frac{g^2 p_1^+}{s}\int_{-\infty}^{\infty}dx_1^-\int_{x_1^-}^{\infty}dx_2^-V_{\underline{x}}[+\infty,x_2^-]t^b\psi_{\beta}(x_2^-,\underline{x})U_{\underline{x}}^{ba}[x_2^-,x_1^-]\left[\frac{1}{2}\gamma^+(1+\sigma\gamma^5)\right]_{\alpha\beta}\\
&\times\bar{\psi}_{\alpha}(x_1^-,\underline{x})t^a V_{\underline{x}}[x_1^-,-\infty].
\end{aligned} \qquad (49)$$

Keeping only the σ-dependent part of the obtained expression we write

$$(V_{\underline{x}}^{\text{pol}})^q = -\frac{g^2 p_1^+}{s}\int_{-\infty}^{\infty}dx_1^-\int_{x_1^-}^{\infty}dx_2^-V_{\underline{x}}[+\infty,x_2^-]t^b\psi_{\beta}(x_2^-,\underline{x})U_{\underline{x}}^{ba}[x_2^-,x_1^-]\left[\frac{1}{2}\gamma^+\gamma^5\right]_{\alpha\beta}\bar{\psi}_{\alpha}(x_1^-,\underline{x})t^a V_{\underline{x}}[x_1^-,-\infty]. \qquad (50)$$

Combining Eqs. (50) and (44) we finally write the full polarized fundamental Wilson line operator as

$$\begin{aligned}
V_{\underline{x}}^{\text{pol}} =\ & \frac{igp_1^+}{s}\int_{-\infty}^{\infty}dx^-V_{\underline{x}}[+\infty,x^-]F^{12}(x^-,\underline{x})V_{\underline{x}}[x^-,-\infty]\\
& -\frac{g^2 p_1^+}{s}\int_{-\infty}^{\infty}dx_1^-\int_{x_1^-}^{\infty}dx_2^-V_{\underline{x}}[+\infty,x_2^-]t^b\psi_{\beta}(x_2^-,\underline{x})U_{\underline{x}}^{ba}[x_2^-,x_1^-]\left[\frac{1}{2}\gamma^+\gamma^5\right]_{\alpha\beta}\bar{\psi}_{\alpha}(x_1^-,\underline{x})t^a V_{\underline{x}}[x_1^-,-\infty].
\end{aligned} \qquad (51)$$

B. Polarized adjoint Wilson line

Let us now repeat the above calculation (along with the calculation from Sec. II B of [13]), but for the adjoint (gluon) polarized Wilson line. Similar to the above, we have to find the high-energy longitudinally polarized gluon scattering amplitude on a longitudinally polarized target, keeping only the polarization-dependent part of the expression.

We begin by considering the scattering amplitude in the left panel of Fig. 6. By analogy to the calculation in [13] we write
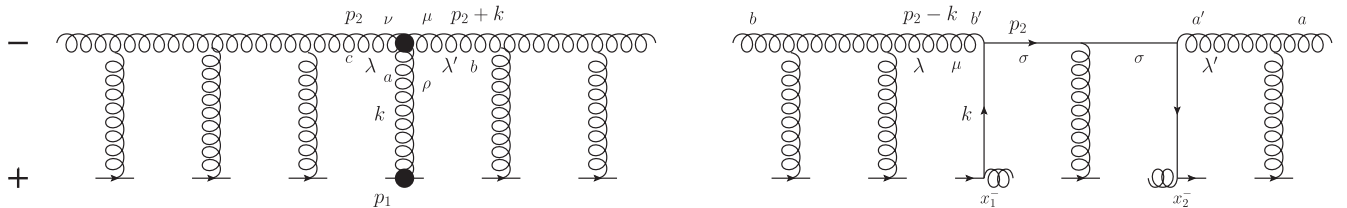
FIG. 6. Two contributions to the polarized adjoint Wilson line in the quasiclassical approximation (in $A^- = 0$ gauge). The filled circles denote the spin-dependent subeikonal scattering.

$$\lambda\delta_{\lambda,\lambda'}\hat{\mathcal{O}}^g_{\text{pol}}(k) \equiv \frac{1}{2p_2^-}\epsilon^{\mu*}_{\lambda'}(p_2+k)[(p_2-k)_\mu g_{\nu\rho}-(2p_2+k)_\rho g_{\mu\nu}+(2k+p_2)_\nu g_{\mu\rho}]\epsilon^\nu_\lambda(p_2)gf^{abc}A^{a\rho}_\perp(k) = \lambda\delta_{\lambda,\lambda'}\frac{g}{p_2^-}\underline{k}\times\underline{\mathcal{A}}(k) \tag{52}$$

with all the indices as labeled in the left panel of Fig. 6. Again we only keep the spin-dependent terms proportional to $\lambda\delta_{\lambda,\lambda'}$, while $\mathcal{A}_\mu$ denotes the color matrix $A^a_\mu T^a$ with T^a the adjoint generators of $\text{SU}(N_c)$. Fourier transforming to coordinate space gives

$$\hat{\mathcal{O}}^g_{\text{pol}}(x^-,\underline{x}) \equiv \int \frac{dk^+}{2\pi}\frac{d^2k}{(2\pi)^2}e^{-ik^+x^-}e^{i\underline{k}\cdot\underline{x}}\left[\frac{g}{p_2^-}\underline{k}\times\underline{\mathcal{A}}(k)\right] = \frac{2}{s}(-igp_1^+)\epsilon^{ij}_T\frac{\partial}{\partial x^i_\perp}\mathcal{A}^j_\perp(x^-,\underline{x}) \equiv \frac{2}{s}(-igp_1^+)\underline{\nabla}\times\underline{\mathcal{A}}(x^-,\underline{x}). \tag{53}$$

We thus obtain the gluon contribution to the polarized adjoint Wilson line

$$(U^{\text{pol}}_{\underline{x}})^g = \frac{2igp_1^+}{s}\int_{-\infty}^{+\infty}dx^- U_{\underline{x}}[+\infty,x^-]\mathcal{F}^{12}(x^+=0,x^-,\underline{x})U_{\underline{x}}[x^-,-\infty], \tag{54}$$

where $\mathcal{F}^{12}$ is the component of the field-strength tensor in the adjoint representation and

$$U_{\underline{x}}[b^-,a^-] = \mathcal{P}\exp\left[ig\int_{a^-}^{b^-}dx^-\mathcal{A}^+(x^+=0,x^-,\underline{x})\right] \tag{55}$$

is the adjoint Wilson line.

Finally, defining a rescaled gluon field

$$\underline{\mathcal{A}}(x^-,\underline{x}) = \frac{S_L}{2p_1^+}\underline{\bar{\mathcal{A}}}(x^-,\underline{x}) \tag{56}$$

we obtain

$$(U^{\text{pol}}_{\underline{x}})^g = \frac{1}{s}\int_{-\infty}^{\infty}dx^- U_{\underline{x}}[+\infty,x^-]\left(-ige^{ij}_T\frac{\partial}{\partial x^i_\perp}\bar{\mathcal{A}}^j_\perp(x^-,\underline{x})\right)U_{\underline{x}}[x^-,-\infty] = \frac{ig}{s}\int_{-\infty}^{\infty}dx^- U_{\underline{x}}[+\infty,x^-]\bar{\mathcal{F}}^{12}(x^-,\underline{x})U_{\underline{x}}[x^-,-\infty]. \tag{57}$$

Now let us consider the contribution of quark t-channel exchanges, as shown in the right panel of Fig. 6. Starting with the exchange on the left we write for it

$$\frac{1}{2p_2^-}ig\bar{u}_\sigma(p_2)t^{b'}\gamma^\mu\psi(k)\epsilon^\mu_\lambda(p_2-k) = -\frac{ig}{\sqrt{\sqrt{2}p_2^-}}\delta_{\sigma,\lambda}\rho^T(\sigma)t^{b'}\gamma^0\psi(k). \tag{58}$$

In coordinate space we have

$$-\frac{ig}{\sqrt{\sqrt{2}p_2^-}}\delta_{\sigma,\lambda}\rho^T(\sigma)t^{b'}\gamma^0\psi(x_1^-,\underline{x}). \tag{59}$$

The right t-channel quark exchange in the right panel of Fig. 6 yields

$$-\frac{ig}{\sqrt{\sqrt{2}p_2^-}}\delta_{\sigma,\lambda'}\bar{\psi}(x_2^-,\underline{x})t^{a'}\rho(\sigma). \tag{60}$$

Combining these results together we write

$$
\lambda \delta_{\lambda\lambda'}(U_{\underline{x}}^{\mathrm{pol}})^{q\,ab} \supset -\frac{g^2}{\sqrt{2}p_2^-}\delta_{\lambda\lambda'}\left[\int_{-\infty}^{\infty}dx_1^-\int_{x_1^-}^{\infty}dx_2^- U_{\underline{x}}^{aa'}[+\infty,x_2^-]\bar{\psi}(x_2^-,\underline{x})t^{a'}\rho(\lambda)V_{\underline{x}}[x_2^-,x_1^-]\right.
$$

$$
\times \rho^T(\lambda)t^{b'}\gamma^0\psi(x_1^-,\underline{x})U_{\underline{x}}^{b'b}[x_1^-,-\infty]+\int_{-\infty}^{\infty}dx_1^-\int_{-\infty}^{x_1^-}dx_2^- U_{\underline{x}}^{ab'}[+\infty,x_1^-]\bar{\psi}(x_2^-,\underline{x})t^{a'}\rho(\lambda)V_{\underline{x}}[x_2^-,x_1^-]
$$

$$
\left.\times \rho^T(\lambda)t^{b'}\gamma^0\psi(x_1^-,\underline{x})U_{\underline{x}}^{a'b}[x_2^-,-\infty]\right]
$$

$$
=-\frac{g^2}{\sqrt{2}p_2^-}\delta_{\lambda\lambda'}\int_{-\infty}^{\infty}dx_1^-\int_{x_1^-}^{\infty}dx_2^- U_{\underline{x}}^{aa'}[+\infty,x_2^-][\bar{\psi}(x_2^-,\underline{x})t^{a'}\rho(\lambda)V_{\underline{x}}[x_2^-,x_1^-]
$$

$$
\times \rho^T(\lambda)t^{b'}\gamma^0\psi(x_1^-,\underline{x})+\mathrm{c.c.}]U_{\underline{x}}^{b'b}[x_1^-,-\infty] \tag{61}
$$

where the second term in the brackets is due to the contribution of the diagram in which the quark particle number flows in an opposite direction from that in the right panel of Fig. 6. Simplifying further we arrive at

$$
\lambda\delta_{\lambda\lambda'}(U_{\underline{x}}^{\mathrm{pol}})^{q\,ab} \supset -\frac{g^2}{2p_2^-}\delta_{\lambda\lambda'}\int_{-\infty}^{\infty}dx_1^-\int_{x_1^-}^{\infty}dx_2^- U_{\underline{x}}^{aa'}[+\infty,x_2^-]\left\{\bar{\psi}_\alpha(x_2^-,\underline{x})t^{a'}V_{\underline{x}}[x_2^-,x_1^-]\left[\frac{1}{2}\gamma^+(1+\lambda\gamma_5)\right]_{\alpha\beta}\right.
$$

$$
\left.\times t^{b'}\psi_\beta(x_1^-,\underline{x})+\mathrm{c.c.}\right\}U_{\underline{x}}^{b'b}[x_1^-,-\infty]. \tag{62}
$$

Finally, keeping only the λ-dependent term we arrive at the expression for the adjoint polarized Wilson line with quark exchanges in the t-channel:

$$
(U_{\underline{x}}^{\mathrm{pol}})^{q\,ab} = -\frac{g^2 p_1^+}{s}\int_{-\infty}^{\infty}dx_1^-\int_{x_1^-}^{\infty}dx_2^- U_{\underline{x}}^{aa'}[+\infty,x_2^-]\left\{\bar{\psi}_\alpha(x_2^-,\underline{x})t^{a'}V_{\underline{x}}[x_2^-,x_1^-]\left[\frac{1}{2}\gamma^+\gamma_5\right]_{\alpha\beta}\right.
$$

$$
\left.\times t^{b'}\psi_\beta(x_1^-,\underline{x})+\mathrm{c.c.}\right\}U_{\underline{x}}^{b'b}[x_1^-,-\infty]. \tag{63}
$$

With the help of Eqs. (54) and (63) we derive the full adjoint polarized Wilson line operator:

$$
(U_{\underline{x}}^{\mathrm{pol}})^{ab} = \frac{2igp_1^+}{s}\int_{-\infty}^{+\infty}dx^-(U_{\underline{x}}[+\infty,x^-]\mathcal{F}^{12}(x^+=0,x^-,\underline{x})U_{\underline{x}}[x^-,-\infty])^{ab}
$$

$$
-\frac{g^2 p_1^+}{s}\int_{-\infty}^{\infty}dx_1^-\int_{x_1^-}^{\infty}dx_2^- U_{\underline{x}}^{aa'}[+\infty,x_2^-]\bar{\psi}(x_2^-,\underline{x})t^{a'}V_{\underline{x}}[x_2^-,x_1^-]\frac{1}{2}\gamma^+\gamma_5 t^{b'}\psi(x_1^-,\underline{x})U_{\underline{x}}^{b'b}[x_1^-,-\infty]-\mathrm{c.c.} \tag{64}
$$

IV. SMALL-x HELICITY EVOLUTION AT LARGE-N_c

We are now ready to use the polarized Wilson line operators derived above to cross-check the small-x helicity evolution equations derived in [9–13]. Those equations close only in the large-N_c and the larger-N_c and N_f limits. We begin with the large-N_c limit, which is dominated by gluons.

We are interested in the evolution of the adjoint polarized dipole amplitude, defined by

$$
G_{10}^{\mathrm{adj}}(zs) = \frac{1}{2(N_c^2-1)}\mathrm{Re}\langle\langle\mathrm{TTr}[U_{\underline{0}}(U_{\underline{1}}^{\mathrm{pol}g})^\dagger]+\mathrm{TTr}[U_{\underline{1}}^{\mathrm{pol}g}U_{\underline{0}}^\dagger]\rangle\rangle
$$

$$
\equiv \frac{zs}{2(N_c^2-1)}\mathrm{Re}\langle\mathrm{TTr}[U_{\underline{0}}(U_{\underline{1}}^{\mathrm{pol}g})^\dagger]+\mathrm{TTr}[U_{\underline{1}}^{\mathrm{pol}g}U_{\underline{0}}^\dagger]\rangle
$$

$$
= \frac{p^+}{N_c^2-1}\int_{-\infty}^{\infty}dx_1^-\mathrm{Re}\left\langle\mathrm{TTr}\left[U_{\underline{0}}U_{\underline{1}}[-\infty,x_1^-]\left(ig\epsilon_T^{ij}\frac{\partial}{\partial(x_1)_\perp^i}\mathcal{A}_\perp^j(x_1^-,\underline{x}_1)\right)U_{\underline{1}}[x_1^-,\infty]\right]+\mathrm{c.c.}\right\rangle(zs). \tag{65}
$$

Here Tr denotes a color trace in the adjoint representation. We are keeping only the gluon operator contribution to the polarized Wilson lines. The diagrams giving the DLA large-N_c evolution of $G_{10}^{\text{adj}}(zs)$ are in complete analogy with the Fig. 2 of [13]. They are shown in Fig. 7 here. In the large-N_c limit quark loops are suppressed. Therefore, the soft quark emission is not included (cf. Fig. 8 below). For brevity, from now on we will often omit the Re sign, implying that it is applied to all of the correlators below.

Employing the notation from [13] we write

$$(\delta G_{10}^{adj})_{\text{I}} = \frac{g^2 p^+}{N_c^2 - 1} \int\limits_{-\infty}^{0} dx_1^- \int\limits_{0}^{\infty} dx_2^- \left\langle \text{T Tr} \left[U_{\underline{0}} T^a U_{\underline{1}}^\dagger T^b \right] \left(\frac{\partial}{\partial (x_1)_\perp^i} \epsilon_T^{ij} \overline{a_\perp^{j\,a}(x_1^-, \underline{x}_1)} \right) a^{+\,b}(x_2^-, \underline{x}_1) + \text{c.c.} \right\rangle. \tag{66}$$

With the help of the propagator

$$\int\limits_{-\infty}^{0} dx_1^- \int\limits_{0}^{\infty} dx_2^- \left(\frac{\partial}{\partial (x_1)_\perp^i} \epsilon_T^{ij} \overline{a_\perp^{j\,a}(x_1^-, \underline{x}_1)} \right) a^{+\,b}(x_2^-, \underline{x}_1) = \frac{1}{4\pi^3} \int\limits_{0}^{\infty} dk^- \int \frac{d^2 x_2}{x_{21}^2} (U_{\underline{2}}^{pol})_{(k^-)}^{ba}, \tag{67}$$

which was also established in [13], we write
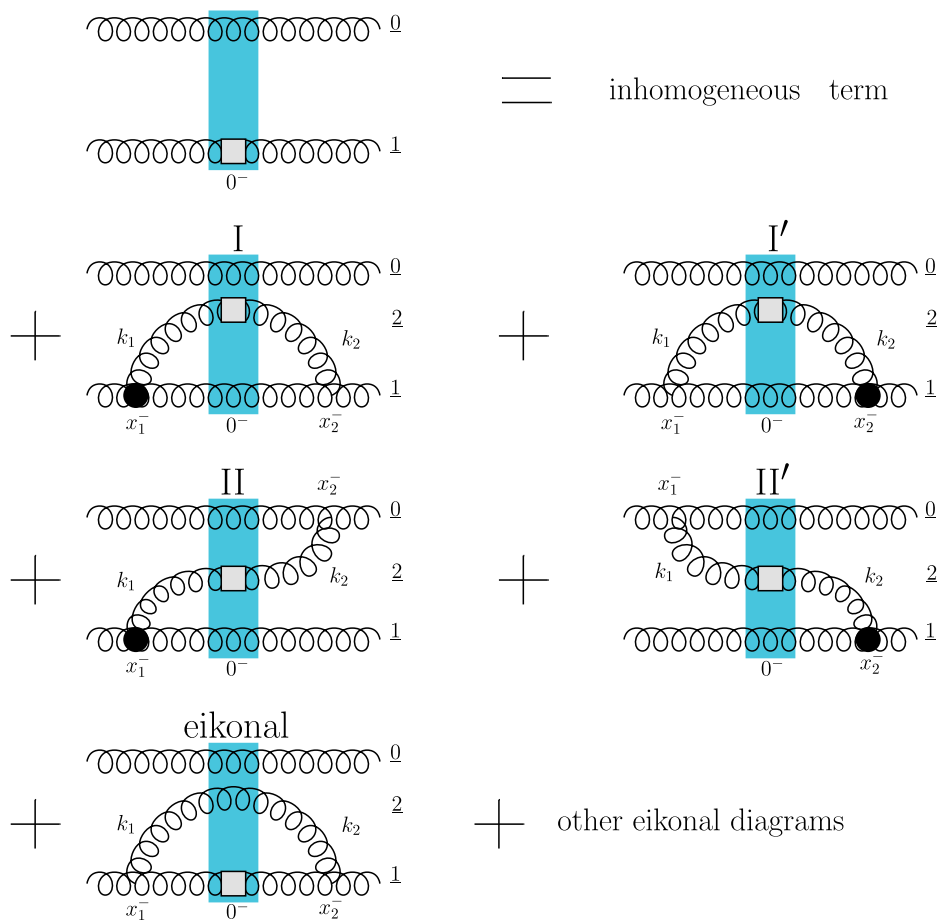
FIG. 7. Diagrams illustrating evolution of the polarized dipole amplitude (65). The blue rectangle represents the target shock wave, the black filled circle represents an insertion of the subeikonal operator (53), and the gray box represents the polarized adjoint Wilson line (57).

$$(\delta G_{10}^{\text{adj}})_{\text{I}}(zs) = \frac{g^2 p^+}{4\pi^3 (N_c^2 - 1)} \int_0^\infty dk^- \int \frac{d^2 x_2}{x_{21}^2} \langle \text{TTr}[U_{\underline{0}} T^a U_{\underline{1}}^\dagger T^b](U_{\underline{2}}^{\text{pol}})^{ba} + \text{c.c.}\rangle (z's = 2p^+ k^-)$$

$$= \frac{\alpha_s}{2\pi^2} \int_{\frac{\Delta^2}{s}}^z \frac{dz'}{z'} \int \frac{d^2 x_2}{x_{21}^2} \left\langle\!\!\left\langle \frac{1}{N_c^2 - 1} \text{TTr}[U_{\underline{0}} T^a U_{\underline{1}}^\dagger T^b](U_{\underline{2}}^{\text{pol}})^{ba} + \text{c.c.}\right\rangle\!\!\right\rangle (z's). \tag{68}$$

Adding the contribution of the diagram I' simply doubles the result, yielding

$$(\delta G_{10}^{\text{adj}})_{\text{I}+\text{I}'}(zs) = \frac{\alpha_s}{2\pi^2} \int_{\frac{\Delta^2}{s}}^z \frac{dz'}{z'} \int \frac{d^2 x_2}{x_{21}^2} \left\langle\!\!\left\langle \frac{2}{N_c^2 - 1} \text{TTr}[U_{\underline{0}} T^a U_{\underline{1}}^\dagger T^b](U_{\underline{2}}^{\text{pol}})^{ba} + \text{c.c.}\right\rangle\!\!\right\rangle (z's). \tag{69}$$

The effect of diagrams II and II' in the DLA is to simply introduce the IR cutoff $x_{10} > x_{21}$ on the x_2 integral in the diagrams I and I' [9,11]. Finally, the "eikonal" diagrams in Fig. 7 are calculated in the same way as for the unpolarized evolution [25–32]. Note that the rescaling in the double angle brackets defined in Eq. (65) is done with the z of the polarized Wilson line, while the z in the argument of the correlator is the longitudinal momentum fraction of the softest line in the dipole [9] (which may be the unpolarized line). In the end we arrive at the following evolution equation for the adjoint polarized dipole amplitude:

$$G_{10}^{\text{adj}}(z) = G_{10}^{\text{adj}(0)}(z) + \frac{\alpha_s}{2\pi^2} \int_{\frac{\Delta^2}{s}}^z \frac{dz'}{z'} \int \frac{d^2 x_2}{x_{21}^2} \theta(x_{10} - x_{21}) \theta\left(x_{21}^2 - \frac{1}{z's}\right)$$

$$\times \left\{ \left\langle\!\!\left\langle \frac{2}{N_c^2 - 1} \text{TTr}[U_{\underline{0}} T^a U_{\underline{1}}^\dagger T^b](U_{\underline{2}}^{\text{pol}})^{ba} + \text{c.c.}\right\rangle\!\!\right\rangle (z') \right.$$

$$\left. + \frac{1}{N_c^2 - 1} [\langle\langle \text{TTr}[T^b U_{\underline{0}} T^a U_{\underline{1}}^{\text{pol}\dagger}] U_{\underline{2}}^{ba}\rangle\rangle (z') - N_c \langle\langle \text{TTr}[U_{\underline{0}} U_{\underline{1}}^{\text{pol}\dagger}]\rangle\rangle (z') + \text{c.c.}]\right\}. \tag{70}$$

[We have suppressed the s in zs in the arguments of the functions and correlators in (70).] The evolution equation (70) is consistent with Eq. (62) from [9] and with Eq. (A1) in [11].

Next let us take the large-N_c limit of Eq. (70). This means rewriting (70) in terms of the fundamental polarized dipole amplitudes. Start with the true (unpolarized) adjoint Wilson line

$$(U_{\underline{0}})^{ab} = 2\text{tr}[t^b V_{\underline{0}}^\dagger t^a V_{\underline{0}}]. \tag{71}$$

To derive a similar relation for $(U^{\text{pol}})^g$ from Eq. (57) we write

$$(U_{\underline{x}}^{\text{pol}})^{g\,ab} = \frac{ig}{s} \int_{-\infty}^\infty dx^- (U_{\underline{x}}[+\infty, x^-])^{ac} (T^e)^{cd} (U_{\underline{x}}[x^-, -\infty])^{db} \bar{F}^{e12}(x^-, \underline{x})$$

$$= \frac{4g}{s} \int_{-\infty}^\infty dx^- \text{tr}[t^c V_{\underline{x}}^\dagger[+\infty, x^-] t^a V_{\underline{x}}[+\infty, x^-]] f^{ecd} \text{tr}[t^b V_{\underline{x}}^\dagger[x^-, -\infty] t^d V_{\underline{x}}[x^-, -\infty]] \bar{F}^{e12}(x^-, \underline{x})$$

$$= \frac{-8ig}{s} \int_{-\infty}^\infty dx^- \text{tr}[t^c V_{\underline{x}}^\dagger[+\infty, x^-] t^a V_{\underline{x}}[+\infty, x^-]] \text{tr}[t^c[t^d, t^e]] \text{tr}[t^b V_{\underline{x}}^\dagger[x^-, -\infty] t^d V_{\underline{x}}[x^-, -\infty]] \bar{F}^{e12}(x^-, \underline{x})$$

$$= \frac{-4ig}{s} \int_{-\infty}^\infty dx^- \text{tr}[V_{\underline{x}}^\dagger[+\infty, x^-] t^a V_{\underline{x}}[+\infty, x^-] [t^d, t^e]] \text{tr}[t^b V_{\underline{x}}^\dagger[x^-, -\infty] t^d V_{\underline{x}}[x^-, -\infty]] \bar{F}^{e12}(x^-, \underline{x})$$

$$= \frac{-2ig}{s} \int_{-\infty}^\infty dx^- \bar{F}^{e12}(x^-, \underline{x}) \{\text{tr}[t^e V_{\underline{x}}^\dagger[+\infty, x^-] t^a V_{\underline{x}}[+\infty, x^-] V_{\underline{x}}[x^-, -\infty] t^b V_{\underline{x}}^\dagger[x^-, -\infty]]$$

$$- \text{tr}[V_{\underline{x}}^\dagger[+\infty, x^-] t^a V_{\underline{x}}[+\infty, x^-] t^e V_{\underline{x}}[x^-, -\infty] t^b V_{\underline{x}}^\dagger[x^-, -\infty]]\}. \tag{72}$$

The expression for the polarized fundamental Wilson line is given by Eq. (44), which for the momentum-rescaled gluon field reads

$$(V_{\underline{x}}^{\text{pol}})^g = \frac{ig}{2s} \int_{-\infty}^\infty dx^- V_{\underline{x}}[+\infty, x^-] t^e \bar{F}^{e12}(x^-, \underline{x}) V_{\underline{x}}[x^-, -\infty]. \tag{73}$$

With the help of Eq. (73) we rewrite Eq. (72) as [cf. Eq. (71)]

$$(U_{\underline{x}}^{\text{pol}})^{gab} = 4\text{tr}[V_{\underline{x}}^{\text{pol}\dagger}t^a V_{\underline{x}}t^b] + 4\text{tr}[V_{\underline{x}}^{\dagger}t^a V_{\underline{x}}^{\text{pol}}t^b]. \quad (74)$$

This is twice larger than Eq. (A5) in the Appendix A of [11]. The latter equation was only conjectured in [11] and the coefficient in it was not derived or cross-checked. Since (for $N_f = 0$) all the evolution equations are linear in U^{pol}, our end result (A12) in the same Appendix A of [11] would not change from multiplying all U^{pol} in the starting point (A1) in [11] by a constant.

Define the fundamental polarized dipole amplitude with only the gluon operator contributing to the fundamental polarized Wilson lines [cf. Eq. (28)]

$$G_{10}(z) = \frac{1}{2N_c}\text{Re}\langle\!\langle\text{Ttr}[V_0(V_1^{\text{pol}\,g})^{\dagger}] + \text{Ttr}[V_1^{\text{pol}\,g}V_0^{\dagger}]\rangle\!\rangle. \quad (75)$$

With the help of Eq. (74) we can see that at large N_c

$$G_{10}^{\text{adj}}(z) = 4G_{10}(z). \quad (76)$$

The coefficient 4 of the right of Eq. (76) is twice larger than the more familiar coefficient 2 in the unpolarized version of this relation.

Repeating all the trace algebra from the Appendix A of [11] with Eqs. (71) and (74) defining the unpolarized (normal) and the polarized Wilson lines respectively (instead of (A3) and (A5) of [11]), yields

$$G_{10}(z) = G_{10}^{(0)}(z) + \frac{\alpha_s N_c}{2\pi}\int_{\frac{1}{sx_{10}^2}}^{z}\frac{dz'}{z'}\int_{\frac{1}{z's}}^{x_{10}^2}\frac{dx_{21}^2}{x_{21}^2}$$
$$\times [\Gamma_{10,21}(z') + 3G_{21}(z')], \quad (77)$$

in complete agreement with the equation derived in [9]. (See the next section for details of this transition.) Here $\Gamma_{10,21}$ is defined operatorially by the same Eq. (75), but with the dipole size ordering on the subsequent evolution being dependent on the size x_{21} of another dipole [9]. We refer to $\Gamma_{10,21}$ as the "neighbor" dipole amplitude. Its evolution equation is similar to that of G_{10},

$$\Gamma_{10,21}(z') = \Gamma_{10,21}^{(0)}(z') + \frac{\alpha_s N_c}{2\pi}\int_{\min\{\Lambda^2,\frac{1}{x_{10}^2}\}/s}^{z'}\frac{dz''}{z''}\int_{\frac{1}{z''s}}^{\min\{x_{10}^2,x_{21}^2 z'/z''\}}\frac{dx_{32}^2}{x_{32}^2}[\Gamma_{10,32}(z'') + 3G_{32}(z'')], \quad (78)$$

and also follows from our operator approach. This result is also in agreement with [9].

In [13] we have already constructed the evolution equation for the fundamental polarized dipole amplitude using the operator formalism and anticipating the large-N_c limit. The result is given by Eq. (74) in [13], which reads

$$G_{10}(zs) = G_{10}^{(0)}(zs) + \frac{\alpha_s N_c}{2\pi}\int_{\frac{\Lambda^2}{s}}^{z}\frac{dz'}{z'}\int_{1/(z's)}^{x_{10}^2}\frac{dx_{21}^2}{x_{21}^2}\left\{\left\langle\!\left\langle\frac{1}{N_c^2}\text{Ttr}[V_{\underline{0}}t^a V_{\underline{1}}^{\dagger}t^b](U_{\underline{2}}^{\text{pol}})^{ba} + \text{c.c.}\right\rangle\!\right\rangle(z's)\right.$$
$$\left. + \left\langle\!\left\langle\frac{1}{N_c^2}\text{Ttr}[V_{\underline{0}}t^a V_{\underline{1}}^{\text{pol}\dagger}t^b](U_{\underline{2}})^{ba} - \frac{C_F}{N_c^2}\text{Ttr}[V_{\underline{0}}V_{\underline{1}}^{\text{pol}\dagger}] + \text{c.c.}\right\rangle\!\right\rangle(z's)\right\}. \quad (79)$$

Using Eq. (74) along with

$$\langle\!\langle\text{tr}[V_{\underline{0}}t^a V_{\underline{1}}^{\dagger}t^b](U_{\underline{2}}^{\text{pol}})^{ba}\rangle\!\rangle = N_c\langle\!\langle\text{tr}[V_{\underline{0}}V_{\underline{2}}^{\text{pol}\dagger}]\rangle\!\rangle + N_c\langle\!\langle\text{tr}[V_{\underline{2}}^{\text{pol}}V_{\underline{1}}^{\dagger}]\rangle\!\rangle + \mathcal{O}\left(\frac{1}{N_c}\right) \quad (80)$$

we take the large-N_c limit of Eq. (79) obtaining

$$G_{10}(zs) = G_{10}^{(0)}(zs) + \frac{\alpha_s N_c}{2\pi^2}\int_{\frac{\Lambda^2}{s}}^{z}\frac{dz'}{z'}\int\frac{d^2x_2}{x_{21}^2}\theta(x_{10}^2 - x_{21}^2)\theta\left(x_{21}^2 - \frac{1}{z's}\right)\left\{\left\langle\!\left\langle\frac{1}{N_c}\text{Ttr}[V_{\underline{0}}V_{\underline{2}}^{\text{pol}\dagger}]\right.\right.\right.$$
$$\left.\left.\left. + \frac{1}{N_c}\text{Ttr}[V_{\underline{2}}^{\text{pol}}V_{\underline{1}}^{\dagger}] + \text{c.c.}\right\rangle\!\right\rangle(z's) + \left\langle\!\left\langle\frac{1}{2N_c}\text{Ttr}[V_{\underline{2}}V_{\underline{1}}^{\text{pol}\dagger}] - \frac{1}{2N_c}\text{Ttr}[V_{\underline{0}}V_{\underline{1}}^{\text{pol}\dagger}] + \text{c.c.}\right\rangle\!\right\rangle(z's)\right\}, \quad (81)$$

in agreement with Eq. (77) from [13]. In turn, Eq. (81) leads to above Eqs. (77) and (78) for the polarized dipole amplitude and for the neighbor dipole amplitude.

V. SMALL-x HELICITY EVOLUTION AT LARGE-N_c AND N_f

Now let us rederive helicity evolution equations in the large-N_c and N_f limit using the operators obtained here. Just like in Sec. IV, we start with the evolution of the adjoint polarized dipole amplitude, now defined by including the full U^{pol} from Eq. (64):

$$G_{10}^{\text{adj}}(zs) = \frac{1}{2(N_c^2-1)} \text{Re} \langle\!\langle \text{TTr}[U_{\underline{0}} U_{\underline{1}}^{\text{pol}\dagger}] + \text{TTr}[U_{\underline{1}}^{\text{pol}} U_{\underline{0}}^{\dagger}] \rangle\!\rangle$$

$$= \frac{p^+}{N_c^2-1} \int_{-\infty}^{\infty} dx_1^- \text{Re} \left\langle \text{TTr} \left[U_{\underline{0}} U_1[-\infty, x_1^-] \left(ig\epsilon_T^{ij} \frac{\partial}{\partial(x_1)_\perp^i} \mathcal{A}_\perp^j(x_1^-, \underline{x}_1) \right) U_1[x_1^-, \infty] \right] + \text{c.c.} \right\rangle (zs)$$

$$- \frac{g^2 p^+}{2(N_c^2-1)} \int_{-\infty}^{\infty} dx_1^- \int_{x_1^-}^{\infty} dx_2^- \text{Re} \left\langle \text{T}(U_{\underline{0}}^{\dagger})^{ba} U_{\underline{1}}^{aa'}[+\infty, x_2^-] \left\{ \bar{\psi}(x_2^-, \underline{x}_1) t^{a'} V_{\underline{1}}[x_2^-, x_1^-] \frac{1}{2} \gamma^+ \gamma_5 t^{b'} \psi(x_1^-, \underline{x}_1) + \text{c.c.} \right\} \right.$$

$$\times U_{\underline{1}}^{b'b}[x_1^-, -\infty] + \text{c.c.} \left\rangle (zs). \right. \tag{82}$$

One can further simplify the quark contribution to the polarized adjoint Wilson line:

$$(U_{\underline{x}}^{\text{pol}})^{q\,ab} = -\frac{g^2 p_1^+}{s} \int_{-\infty}^{\infty} dx_1^- \int_{x_1^-}^{\infty} dx_2^- U_{\underline{x}}^{aa'}[+\infty, x_2^-] \left\{ \bar{\psi}(x_2^-, \underline{x}) t^{a'} V_{\underline{x}}[x_2^-, x_1^-] \frac{1}{2} \gamma^+ \gamma_5 t^{b'} \psi(x_1^-, \underline{x}) + \text{c.c.} \right\} U_{\underline{x}}^{b'b}[x_1^-, -\infty]$$

$$= -\frac{g^2 p_1^+}{s} \int_{-\infty}^{\infty} dx_1^- \int_{x_1^-}^{\infty} dx_2^- \bar{\psi}(x_2^-, \underline{x}) V_{\underline{x}}[x_2^-, +\infty] t^a V_{\underline{x}} \frac{1}{2} \gamma^+ \gamma_5 t^b V_{\underline{x}}[-\infty, x_1^-] \psi(x_1^-, \underline{x}) + \text{c.c.}$$

$$= -\frac{g^2 p_1^+}{s} \int_{-\infty}^{\infty} dx_1^- \int_{x_1^-}^{\infty} dx_2^- \text{tr} \left[t^a V_{\underline{x}} t^b \left(V_{\underline{x}}[+\infty, x_2^-] \psi(x_2^-, \underline{x})_\alpha \left(\frac{1}{2} \gamma^+ \gamma_5 \right)_{\beta\alpha} \bar{\psi}(x_1^-, \underline{x})_\beta V_{\underline{x}}[x_1^-, -\infty] \right)^\dagger \right] + \text{c.c.}. \tag{83}$$

However, it turns out that a relation similar to Eq. (74) connecting the polarized adjoint and fundamental Wilson lines is not easy to obtain in the large-N_c and N_f limit. Instead, we will turn our attention to the polarized dipole amplitudes. Starting with the adjoint amplitude (82), we write using the results of the previous section (after taking the large-N_c and N_f limit in the first term on the right)

$$G_{10}^{\text{adj}}(z) = 4G_{10}(z)$$

$$- \frac{g^2 p^+}{2(N_c^2-1)} \int_{-\infty}^{\infty} dx_1^- \int_{x_1^-}^{\infty} dx_2^- \left\langle \text{T}(U_{\underline{0}}^{\dagger})^{ba} U_{\underline{1}}^{aa'}[+\infty, x_2^-] \left\{ \bar{\psi}(x_2^-, \underline{x}_1) t^{a'} V_{\underline{1}}[x_2^-, x_1^-] \frac{1}{2} \gamma^+ \gamma_5 t^{b'} \psi(x_1^-, \underline{x}_1) + \text{c.c.} \right\} \right.$$

$$\times U_{\underline{1}}^{b'b}[x_1^-, -\infty] + \text{c.c.} \left\rangle (z), \right. \tag{84}$$

where $G_{10}(z)$ is still given by Eq. (75) above. To simplify the second term on the right of Eq. (84) we write

$$(U_{\underline{0}}^{\dagger})^{ba} U_{\underline{1}}^{aa'}[+\infty, x_2^-] \left\{ \bar{\psi}(x_2^-, \underline{x}_1) t^{a'} V_{\underline{1}}[x_2^-, x_1^-] \frac{1}{2} \gamma^+ \gamma_5 t^{b'} \psi(x_1^-, \underline{x}_1) + \text{c.c.} \right\} U_{\underline{1}}^{b'b}[x_1^-, -\infty] + \text{c.c.}$$

$$= U_{\underline{0}}^{ab} \left\{ \bar{\psi}(x_2^-, \underline{x}_1) V_{\underline{1}}[x_2^-, +\infty] t^a V_{\underline{1}} \frac{1}{2} \gamma^+ \gamma_5 t^b V_{\underline{1}}[-\infty, x_1^-] \psi(x_1^-, \underline{x}_1) + \text{c.c.} \right\} + \text{c.c.}$$

$$= U_{\underline{0}}^{ab} \left\{ \text{tr} \left[t^a V_{\underline{1}} t^b \left(V_{\underline{1}}[+\infty, x_2^-] \psi(x_2^-, \underline{x}_1)_\alpha \left(\frac{1}{2} \gamma^+ \gamma_5 \right)_{\beta\alpha} \bar{\psi}(x_1^-, \underline{x}_1)_\beta V_{\underline{1}}[x_1^-, -\infty] \right)^\dagger \right] + \text{c.c.} \right\} + \text{c.c.}$$

$$= \text{tr}[V_{\underline{1}} V_{\underline{0}}^{\dagger}] \text{tr} \left[V_{\underline{0}} \left(V_{\underline{1}}[+\infty, x_2^-] \psi(x_2^-, \underline{x}_1)_\alpha \left(\frac{1}{2} \gamma^+ \gamma_5 \right)_{\beta\alpha} \bar{\psi}(x_1^-, \underline{x}_1)_\beta V_{\underline{1}}[x_1^-, -\infty] \right)^\dagger \right] + \text{c.c.}. \tag{85}$$

Substituting this into Eq. (84), linearizing and taking the large-N_c & N_f limit yields

$$G_{10}^{\text{adj}}(z) = 4G_{10}(z)$$

$$- \frac{g^2 p^+}{2N_c} \int_{-\infty}^{\infty} dx_1^- \int_{x_1^-}^{\infty} dx_2^- \left\langle \text{Ttr} \left[V_{\underline{0}} \left(V_{\underline{1}}[+\infty, x_2^-] \psi(x_2^-, \underline{x}_1)_\alpha \left(\frac{1}{2} \gamma^+ \gamma_5 \right)_{\beta\alpha} \bar{\psi}(x_1^-, \underline{x}_1)_\beta V_{\underline{1}}[x_1^-, -\infty] \right)^\dagger \right] + \text{c.c.} \right\rangle (z). \tag{86}$$

A similar set of operations gives the following expression for the fundamental dipole amplitude (employing the anti-commutativity of the fermion fields):

$$Q_{10}(z) \equiv \frac{1}{2N_c} \mathrm{Re} \left\langle\!\!\left\langle \mathrm{Ttr}[V_{\underline{0}}(V_{\underline{1}}^{\mathrm{pol}})^{\dagger}] + \mathrm{Ttr}[V_{\underline{1}}^{\mathrm{pol}}V_{\underline{0}}^{\dagger}] \right\rangle\!\!\right\rangle$$

$$= G_{10}(z) + \frac{g^2 p^+}{4} \int_{-\infty}^{\infty} dx_1^- \int_{x_1^-}^{\infty} dx_2^- \left\langle \mathrm{T}\bar{\psi}(x_1^-,\underline{x}_1) V_{\underline{1}}[x_1^-,x_2^-] \frac{1}{2}\gamma^+\gamma_5 \psi(x_2^-,\underline{x}_1) + \mathrm{c.c.} \right\rangle(z). \tag{87}$$

Clearly the objects in Eqs. (86) and (87) are significantly different and should obey different evolution equations.

A. Adjoint polarized dipole evolution

Diagrams contributing to the DLA small-x evolution of the adjoint polarized dipole amplitude in Eq. (82) are shown in Fig. 8. In comparison with Fig. 7 and the large-N_c calculation of the previous Section there are only two new diagrams, the diagrams III and III' in Fig. 8. Their contribution is

$$(\delta G_{10}^{adj})_{\mathrm{III+III'}} = -\frac{g^2 p^+}{2(N_c^2-1)} \int_{-\infty}^{0} dx_1^- \int_{0}^{\infty} dx_2^-$$

$$\times \left\langle \mathrm{T}\,(U_{\underline{0}})^{ab} \left\{ \overline{\vphantom{\psi}\smash{\overline{\psi(x_2^-,\underline{x}_1)\,t^a\,V_{\underline{1}}[\infty,-\infty]}}} \frac{1}{2}\gamma^+\gamma_5\,t^b\,\psi(x_1^-,\underline{x}_1) + \mathrm{c.c.} \right\} \right\rangle(zs) + \mathrm{c.c.}. \tag{88}$$

[The second complex conjugation accounts for the second trace in the polarized dipole amplitude (82): in only doubles the contribution shown explicitly.] Employing Eq. (12) we obtain

$$(\delta G_{10}^{adj})_{\mathrm{III+III'}} = -\frac{g^2 p^+}{N_c^2-1} \int_{-\infty}^{0} dx_1^- \int_{0}^{\infty} dx_2^- \left\langle \mathrm{T}(U_{\underline{0}})^{ab}(t^a V_{\underline{1}} t^b)^{ij} \int d^2w \frac{d^2k_1 dk_1^-}{(2\pi)^3 (2k_1^-)^2} \frac{d^2k_2}{(2\pi)^2} e^{i\frac{k_1^2}{2k_1^-}x_1^- + i\underline{k}_1\cdot(\underline{w}-\underline{x}_1)} \right.$$

$$\times \left. e^{-i\frac{k_2^2}{2k_1^-}x_2^- + i\underline{k}_2\cdot(\underline{x}_1-\underline{w})} \theta(k_1^-) \mathrm{tr}\left[\frac{1}{2}\gamma^+\gamma_5 \slashed{k}_1 (\hat{V}_{\underline{w}}^{\dagger})^{ji} \slashed{k}_2 \right] \right\rangle \Bigg|_{k_2^-=k_1^-, k_1^2=0, k_2^2=0} + \mathrm{c.c.} \tag{89}$$

Integrating over x_1^- and x_2^- yields
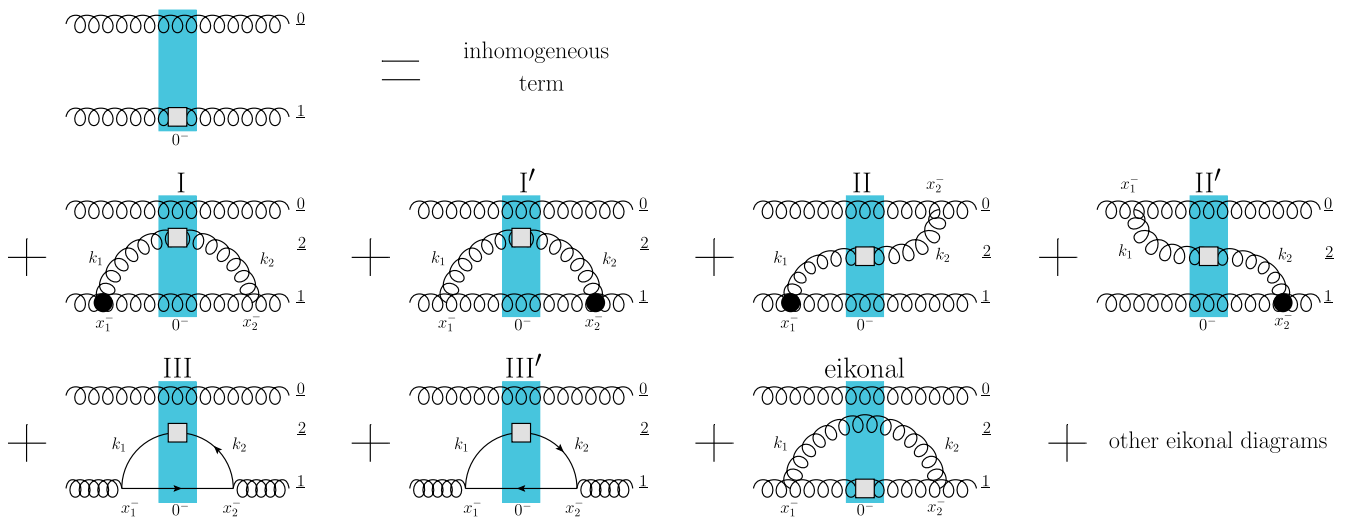
FIG. 8.   Diagrams illustrating evolution of the polarized dipole amplitude (65) at large-N_c and N_f. The blue rectangle represents the classical fields (shock wave), the black vertex represents the sub-eikonal operator insertion (53), and the gray box represents the polarized adjoint or fundamental Wilson line.

$$(\delta G_{10}^{\text{adj}})_{\text{III}+\text{III}'} = \frac{g^2 p^+}{N_c^2 - 1} \left\langle T(U_{\underline{0}})^{ab} (t^a V_{\underline{1}} t^b)^{ij} \int d^2w \frac{d^2k_1 dk_1^-}{(2\pi)^3 \underline{k}_1^2} \frac{d^2k_2}{(2\pi)^2 \underline{k}_2^2} e^{i\underline{k}_1 \cdot (\underline{w}-\underline{x}_1)} e^{i\underline{k}_2 \cdot (\underline{x}_1-\underline{w})} \right.$$

$$\left. \times \theta(k_1^-) \text{tr}\left[\frac{1}{2}\gamma^+\gamma_5 \not{k}_1 (\hat{V}_{\underline{w}}^\dagger)^{ji} \not{k}_2\right] \right\rangle \Bigg|_{k_2^- = k_1^-, k_1^2 = 0, k_2^2 = 0} + \text{c.c.} \tag{90}$$

To evaluate the Dirac matrix trace we have to use polarization sums,

$$\text{tr}\left[\frac{1}{2}\gamma^+\gamma_5 \not{k}_1 (\hat{V}_{\underline{w}}^\dagger)^{ji} \not{k}_2\right] = \sum_{\sigma_1,\sigma_2} \bar{v}_{\sigma_2}(k_2) \frac{1}{2}\gamma^+\gamma_5 v_{\sigma_1}(k_1) \bar{v}_{\sigma_1}(k_1)(\hat{V}_{\underline{w}}^\dagger)^{ji} v_{\sigma_2}(k_2) = 2i\underline{k}_1 \times \underline{k}_2 (V_{\underline{w}}^\dagger)^{ji} - 2\underline{k}_1 \cdot \underline{k}_2 (V_{\underline{w}}^{\text{pol}\dagger})^{ji}, \tag{91}$$

obtaining

$$(\delta G_{10}^{\text{adj}})_{\text{III}+\text{III}'} = -\frac{2g^2 p^+}{N_c^2 - 1} \left\langle T(U_{\underline{0}})^{ab} (t^a V_{\underline{1}} t^b)^{ij} \int d^2w \frac{d^2k_1 dk_1^-}{(2\pi)^3 \underline{k}_1^2} \frac{d^2k_2}{(2\pi)^2 \underline{k}_2^2} e^{i\underline{k}_1 \cdot (\underline{w}-\underline{x}_1)} e^{i\underline{k}_2 \cdot (\underline{x}_1-\underline{w})} \right.$$

$$\left. \times \theta(k_1^-)[-i\underline{k}_1 \times \underline{k}_2 (V_{\underline{w}}^\dagger)^{ji} + \underline{k}_1 \cdot \underline{k}_2 (V_{\underline{w}}^{\text{pol}\dagger})^{ji}] \right\rangle \Bigg|_{k_2^- = k_1^-, k_1^2 = 0, k_2^2 = 0} + \text{c.c.} \tag{92}$$

Fourier-transforming into transverse coordinate space yields

$$(\delta G_{10}^{\text{adj}})_{\text{III}+\text{III}'} = -\frac{\alpha_s N_f}{2\pi^2} \int_{\Lambda^2/s}^1 \frac{dz}{z} \int \frac{d^2w}{|\underline{w}-\underline{x}_1|^2} \frac{1}{N_c^2-1} \langle\langle T(U_{\underline{0}})^{ab} \text{tr}[t^a V_{\underline{1}} t^b V_{\underline{w}}^{\text{pol}\dagger}] + \bar{T}(U_{\underline{0}})^{ab} \text{tr}[V_{\underline{w}}^{\text{pol}} t^b V_{\underline{1}}^\dagger t^a]\rangle\rangle, \tag{93}$$

where we have also inserted a sum over quark flavors. Employing Eq. (71) we get

$$(\delta G_{10}^{\text{adj}})_{\text{III}+\text{III}'} = -\frac{\alpha_s N_f}{2\pi^2} \int_{\Lambda^2/s}^1 \frac{dz}{z} \int \frac{d^2w}{|\underline{w}-\underline{x}_1|^2} \frac{1}{N_c^2-1} \left\langle\left\langle \frac{1}{2} \text{Ttr}[V_{\underline{1}} V_{\underline{0}}^\dagger] \text{tr}[V_{\underline{0}} V_{\underline{w}}^{\text{pol}\dagger}] + \frac{1}{2} \bar{T}\text{tr}[V_{\underline{0}} V_{\underline{1}}^\dagger] \text{tr}[V_{\underline{w}}^{\text{pol}} V_{\underline{0}}^\dagger] \right.\right.$$

$$\left.\left. - \frac{1}{2N_c} \text{Ttr}[V_{\underline{1}} V_{\underline{w}}^{\text{pol}\dagger}] - \frac{1}{2N_c} \bar{T}\text{tr}[V_{\underline{w}}^{\text{pol}} V_{\underline{1}}^\dagger] \right\rangle\right\rangle. \tag{94}$$

Finally, taking the large-N_c and N_f limit and linearizing the equation by neglecting the LLA evolution (which, in practice, means putting the fundamental traces of unpolarized Wilson lines equal to N_c) yields

$$(\delta G_{10}^{\text{adj}})_{\text{III}+\text{III}'} = -\frac{\alpha_s N_f}{2\pi^2} \int_{\Lambda^2/s}^1 \frac{dz}{z} \int \frac{d^2w}{|\underline{w}-\underline{x}_1|^2} \bar{\Gamma}_{\underline{w},\underline{0};\underline{w},\underline{1}}(z) \tag{95}$$

with $\bar{\Gamma}$ being the neighbor polarized dipole amplitude with the polarized line being a true quark, as defined in [9]. (Operatorially $\bar{\Gamma}$ is defined by Eq. (87), by analogy with the neighbor dipole amplitude considered above: again, further evolution of $\bar{\Gamma}$ depends on the size of another dipole [9].)

Adding Eq. (93) to Eq. (70) we obtain

$$G_{10}^{\text{adj}}(z) = G_{10}^{\text{adj}(0)}(z) + \frac{\alpha_s}{2\pi^2} \int_{\frac{\Lambda^2}{s}}^z \frac{dz'}{z'} \int \frac{d^2x_2}{x_{21}^2} \theta\left(x_{21}^2 - \frac{1}{z's}\right)$$

$$\times \left\{ \theta(x_{10} - x_{21}) \left\langle\left\langle \frac{2}{N_c^2-1} \text{TTr}[U_{\underline{0}} T^a U_{\underline{1}}^\dagger T^b](U_{\underline{2}}^{\text{pol}})^{ba} + \text{c.c.} \right\rangle\right\rangle(z') \right.$$

$$+ \theta(x_{10} - x_{21}) \frac{1}{N_c^2-1}[\langle\langle \text{TTr}[T^b U_{\underline{0}} T^a U_{\underline{1}}^{\text{pol}\dagger}] U_{\underline{2}}^{ba}\rangle\rangle(z') - N_c\langle\langle \text{TTr}[U_{\underline{0}} U_{\underline{1}}^{\text{pol}\dagger}]\rangle\rangle(z') + \text{c.c.}]$$

$$\left. -\theta(x_{10}^2 z - x_{21}^2 z') \frac{N_f}{N_c^2-1} \langle\langle \text{Ttr}[t^b V_{\underline{1}} t^a V_{\underline{2}}^{\text{pol}\dagger}] U_{\underline{0}}^{ba} + \bar{T}\text{tr}[t^b V_{\underline{2}}^{\text{pol}} t^a V_{\underline{1}}^\dagger] U_{\underline{0}}^{ba}\rangle\rangle(z') \right\} \tag{96}$$

in agreement with Eq. (A1) of [11].

Using Eq. (95) we rewrite this equation as

$$
G_{10}^{\text{adj}}(z) = G_{10}^{\text{adj}(0)}(z) + \frac{\alpha_s}{2\pi^2} \int_{\Lambda^2/s}^{z} \frac{dz'}{z'} \int \frac{d^2 x_2}{x_{21}^2} \theta\left(x_{21}^2 - \frac{1}{z's}\right) \left\{ \theta(x_{10} - x_{21}) \left\langle\!\!\left\langle \frac{2}{N_c^2 - 1} \text{TTr}[U_{\underline{0}} T^a U_{\underline{1}}^{\dagger} T^b](U_{\underline{2}}^{\text{pol}})^{ba} + \text{c.c.} \right\rangle\!\!\right\rangle(z')
$$
$$
+ \theta(x_{10} - x_{21}) \frac{1}{N_c^2 - 1} [\langle\!\langle \text{TTr}[T^b U_{\underline{0}} T^a U_{\underline{1}}^{\text{pol}\dagger}] U_{\underline{2}}^{ba} \rangle\!\rangle(z') - N_c \langle\!\langle \text{TTr}[U_{\underline{0}} U_{\underline{1}}^{\text{pol}\dagger}] \rangle\!\rangle(z') + \text{c.c.}] \Big\}
$$
$$
- \frac{\alpha_s N_f}{2\pi} \int_{\Lambda^2/s}^{z} \frac{dz'}{z'} \int_{1/(z's)}^{x_{10}^2 z/z'} \frac{dx_{21}^2}{x_{21}^2} \bar{\Gamma}_{20;21}(z'), \tag{97}
$$

where we anticipate the linearized approximation by neglecting LLA terms. Let us reiterate that $\bar{\Gamma}$ is defined as in Eq. (87) but for the neighbor dipole amplitude.

To evaluate the rest of Eq. (97) we employ the definition (64) of the polarized Wilson line. A little algebra involving multiple use of Fierz identity yields

$$
\frac{1}{N_c^2 - 1} \langle\!\langle \text{TTr}[T^b U_{\underline{0}} T^a U_{\underline{1}}^{\dagger}](U_{\underline{2}}^{\text{pol}})^{ba} \rangle\!\rangle(z) = \frac{N_c}{2} G_{21}^{\text{adj}}(z) + \frac{N_c}{2} \Gamma_{20,21}^{\text{adj}}(z) + \mathcal{O}\left(\frac{1}{N_c}\right), \tag{98}
$$

where $\Gamma_{02,21}^{\text{adj}}$ is defined just like G^{adj} in Eq. (82), but for the neighbor adjoint dipole.

Similarly, one can show that

$$
\frac{1}{N_c^2 - 1} \langle\!\langle \text{TTr}[T^b U_{\underline{0}} T^a U_{\underline{1}}^{\text{pol}\dagger}] U_{\underline{2}}^{ba} \rangle\!\rangle(z) = \frac{N_c}{2} G_{21}^{\text{adj}}(z) + \frac{N_c}{2} \Gamma_{10,21}^{\text{adj}}(z) + \mathcal{O}\left(\frac{1}{N_c}\right). \tag{99}
$$

Employing these results in Eq. (97) we obtain in the DLA,

$$
G_{10}^{\text{adj}}(z) = G_{10}^{\text{adj}(0)}(z) + \frac{\alpha_s N_c}{2\pi} \int_{\max\{\Lambda^2, 1/x_{10}^2\}/s}^{z} \frac{dz'}{z'} \int_{1/(z's)}^{x_{10}^2} \frac{dx_{21}^2}{x_{21}^2} [\Gamma_{10,21}^{\text{adj}}(z') + 3 G_{21}^{\text{adj}}(z')]
$$
$$
- \frac{\alpha_s N_f}{2\pi} \int_{\Lambda^2/s}^{z} \frac{dz'}{z'} \int_{1/(z's)}^{x_{10}^2 z/z'} \frac{dx_{21}^2}{x_{21}^2} \bar{\Gamma}_{10;21}^{\text{gen}}(z'). \tag{100}
$$

In the last term we have replaced $\bar{\Gamma}_{02;21}(z')$ by the "generalized" dipole amplitude (cf. [13])

$$
\bar{\Gamma}_{10;21}^{\text{gen}}(z') = \theta(x_{10} - x_{21}) \bar{\Gamma}_{10;21}(z') + \theta(x_{21} - x_{10}) Q_{21}(z'). \tag{101}
$$

The reason for that is that the neighbor dipole amplitude $\bar{\Gamma}_{20;21}^{\text{gen}}(z')$ is defined (and makes sense in the DLA) only for $x_{21} \gg x_{10} \sim x_{20}$, while the integral in the last term of Eq. (100) includes the region where $x_{21} \sim x_{20} \gg x_{10}$: in that region the two neighbor dipoles 21 and 20 have comparable sizes and the special neighbor amplitude $\bar{\Gamma}$ is no longer needed. It has to be replaced by the "regular" dipole amplitude Q, which is accomplished by defining $\bar{\Gamma}^{\text{gen}}$.

Repeating the above steps for the evolution of an adjoint neighbor dipole we arrive at

$$
\Gamma_{10,21}^{\text{adj}}(z') = \Gamma_{10,21}^{\text{adj}(0)}(z') + \frac{\alpha_s N_c}{2\pi} \int_{\max\{\Lambda^2, 1/x_{10}^2\}/s}^{z'} \frac{dz''}{z''} \int_{1/(z''s)}^{\min\{x_{10}^2, x_{21}^2 z'/z''\}} \frac{dx_{32}^2}{x_{32}^2} [\Gamma_{10,32}^{\text{adj}}(z'') + 3 G_{32}^{\text{adj}}(z'')]
$$
$$
- \frac{\alpha_s N_f}{2\pi} \int_{\Lambda^2/s}^{z'} \frac{dz''}{z''} \int_{1/(z''s)}^{x_{21}^2 z'/z''} \frac{dx_{32}^2}{x_{32}^2} \bar{\Gamma}_{10;32}^{\text{gen}}(z''). \tag{102}
$$

B. Fundamental polarized dipole evolution

Next we have to construct the evolution equations for the fundamental polarized dipole amplitude. In the large-N_c limit the evolution equation was constructed in [13] and is given above in Eq. (79). For the dipole amplitude defined by Eq. (87) it reads
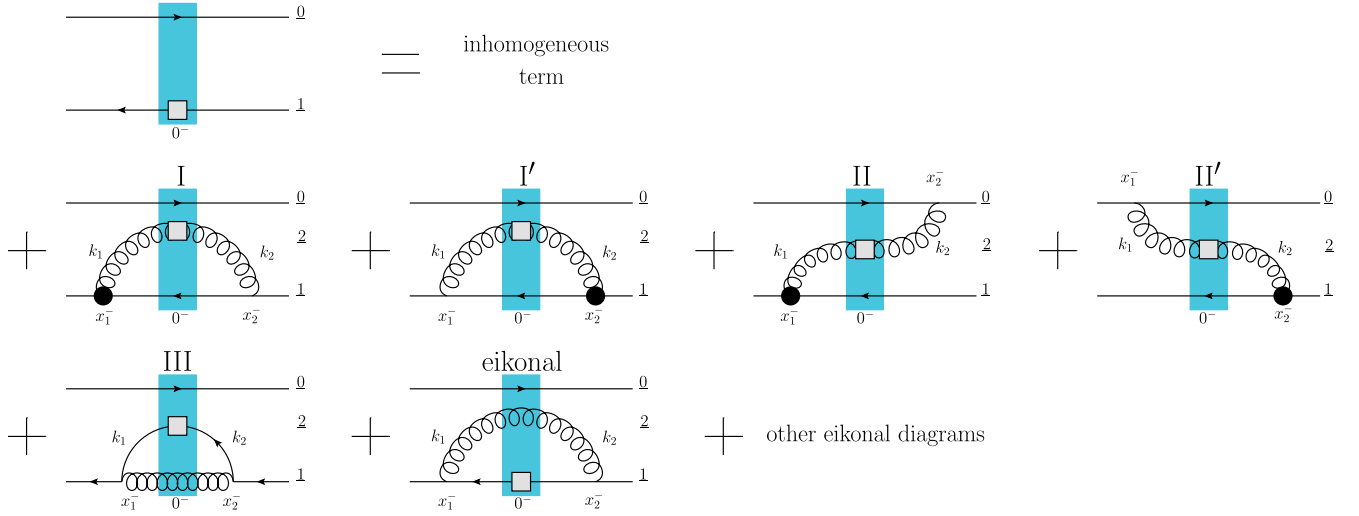
FIG. 9.   Diagrams illustrating evolution of the polarized dipole amplitude (87) at large-N_c and N_f. The notation is the same as in Fig. 8.

$$Q_{10}(zs) = Q_{10}^{(0)}(zs) + \frac{\alpha_s N_c}{2\pi^2} \int_{\frac{\Lambda^2}{s}}^{z} \frac{dz'}{z'} \int \frac{d^2 x_2}{x_{21}^2} \theta(x_{10}^2 - x_{21}^2) \theta\left(x_{21}^2 - \frac{1}{z's}\right) \left\{ \left\langle\!\!\left\langle \frac{1}{N_c^2} \mathrm{Ttr}[V_{\underline{0}} t^a V_{\underline{1}}^\dagger t^b](U_{\underline{2}}^{\mathrm{pol}})^{ba} + \mathrm{c.c.} \right\rangle\!\!\right\rangle(z's) \right.$$

$$\left. + \left\langle\!\!\left\langle \frac{1}{N_c^2} \mathrm{Ttr}[V_{\underline{0}} t^a V_{\underline{1}}^{\mathrm{pol}\dagger} t^b](U_{\underline{2}})^{ba} - \frac{C_F}{N_c^2} \mathrm{Ttr}[V_{\underline{0}} V_{\underline{1}}^{\mathrm{pol}\dagger}] + \mathrm{c.c.} \right\rangle\!\!\right\rangle(z's) \right\} \tag{103}$$

corresponding to all the diagrams on the right of Fig. 9, with the exception of diagram III. For large-N_c and N_f limit this equation needs to be augmented by the contribution of the diagram III in Fig. 9.

Using Eq. (87) we see that the diagram III in Fig. 9 gives

$$(\delta Q_{10}(z))_{\mathrm{III}} = \frac{g^2 p^+}{4} \int_{-\infty}^{0} dx_1^- \int_{0}^{\infty} dx_2^- \left\langle \mathrm{T}\, \overline{\psi}(x_1^-, \underline{x}_1) V_{\underline{1}}[\infty, -\infty] \frac{1}{2} \gamma^+ \gamma_5 \psi(x_2^-, \underline{x}_1) + \mathrm{c.c.} \right\rangle(z). \tag{104}$$

Evaluating the contraction analogous to the above, we get

$$(\delta Q_{10}(z))_{\mathrm{III}} = \frac{\alpha_s}{8\pi^2} \int_{\Lambda^2/s}^{1} \frac{dz}{z} \int \frac{d^2 x_2}{x_{21}^2} \langle\!\langle \mathrm{Ttr}[V_{\underline{1}} V_{\underline{2}}^{\mathrm{pol}\dagger}] + \overline{\mathrm{T}}\mathrm{tr}[V_{\underline{2}}^{\mathrm{pol}} V_{\underline{1}}^\dagger] \rangle\!\rangle(z) = \frac{\alpha_s N_c}{4\pi} \int_{\Lambda^2/s}^{1} \frac{dz}{z} \int \frac{dx_{21}^2}{x_{21}^2} Q_{21}(z). \tag{105}$$

Equation (103) generalized to the case of the large-N_c and N_f limit, now becomes

$$Q_{10}(z) = Q_{10}^{(0)}(zs) + \frac{\alpha_s N_c}{2\pi} \int_{\frac{\Lambda^2}{s}}^{z} \frac{dz'}{z'} \int_{1/(z's)}^{x_{10}^2} \frac{dx_{21}^2}{x_{21}^2} \left\{ \left\langle\!\!\left\langle \frac{1}{N_c^2} \mathrm{Ttr}[V_{\underline{0}} t^a V_{\underline{1}}^\dagger t^b](U_{\underline{2}}^{\mathrm{pol}})^{ba} + \mathrm{c.c.} \right\rangle\!\!\right\rangle(z') \right.$$

$$\left. + \left\langle\!\!\left\langle \frac{1}{N_c^2} \mathrm{Ttr}[V_{\underline{0}} t^a V_{\underline{1}}^{\mathrm{pol}\dagger} t^b](U_{\underline{2}})^{ba} - \frac{C_F}{N_c^2} \mathrm{Ttr}[V_{\underline{0}} V_{\underline{1}}^{\mathrm{pol}\dagger}] + \mathrm{c.c.} \right\rangle\!\!\right\rangle(z') \right\} + \frac{\alpha_s N_c}{4\pi} \int_{\Lambda^2/s}^{z} \frac{dz'}{z'} \int_{1/(z's)}^{x_{10}^2 z/z'} \frac{dx_{21}^2}{x_{21}^2} Q_{21}(z'). \tag{106}$$

Evaluating the terms on the right-hand side of (106) in the large-N_c and linearized limit we get

$$\left\langle\!\!\left\langle \frac{1}{N_c^2} \mathrm{Ttr}[V_{\underline{0}} t^a V_{\underline{1}}^\dagger t^b](U_{\underline{2}}^{\mathrm{pol}})^{ba} + \mathrm{c.c.} \right\rangle\!\!\right\rangle(z') = \frac{1}{2} \Gamma_{20,21}^{\mathrm{adj}}(z') + \frac{1}{2} G_{21}^{\mathrm{adj}}(z') \tag{107}$$

and

$$\left\langle\!\!\left\langle \frac{1}{N_c^2} \mathrm{Ttr}[V_{\underline{0}} t^a V_{\underline{1}}^{\mathrm{pol}\dagger} t^b](U_{\underline{2}})^{ba} - \frac{C_F}{N_c^2} \mathrm{Ttr}[V_{\underline{0}} V_{\underline{1}}^{\mathrm{pol}\dagger}] + \mathrm{c.c.} \right\rangle\!\!\right\rangle(z') = Q_{21}(z') - \overline{\Gamma}_{10,21}(z'). \tag{108}$$

Substituting Eqs. (107) and (108) back into Eq. (106) and applying the standard DLA simplifications yields

$$Q_{10}(z) = Q_{10}^{(0)}(z) + \frac{\alpha_s N_c}{2\pi} \int_{\frac{\Lambda^2}{s}}^{z} \frac{dz'}{z'} \int_{1/(z's)}^{x_{10}^2} \frac{dx_{21}^2}{x_{21}^2} \left\{ \frac{1}{2} \Gamma_{10,21}^{\mathrm{adj}}(z') + \frac{1}{2} G_{21}^{\mathrm{adj}}(z') + Q_{21}(z') - \bar{\Gamma}_{10,21}(z') \right\}$$
$$+ \frac{\alpha_s N_c}{4\pi} \int_{\Lambda^2/s}^{z} \frac{dz'}{z'} \int_{1/(z's)}^{x_{10}^2 z/z'} \frac{dx_{21}^2}{x_{21}^2} Q_{21}(z'). \tag{109}$$

Similarly, for the neighbor dipole amplitude we write

$$\bar{\Gamma}_{10,21}(z') = \bar{\Gamma}_{10,21}^{(0)}(z') + \frac{\alpha_s N_c}{2\pi} \int_{\frac{\Lambda^2}{s}}^{z'} \frac{dz''}{z''} \int_{1/(z''s)}^{\min\{x_{10}^2, x_{21}^2 z'/z''\}} \frac{dx_{32}^2}{x_{32}^2} \left\{ \frac{1}{2} \Gamma_{10,32}^{\mathrm{adj}}(z'') + \frac{1}{2} G_{32}^{\mathrm{adj}}(z'') + Q_{32}(z'') - \bar{\Gamma}_{10,32}(z'') \right\}$$
$$+ \frac{\alpha_s N_c}{4\pi} \int_{\Lambda^2/s}^{z'} \frac{dz''}{z''} \int_{1/(z''s)}^{x_{21}^2 z/z'} \frac{dx_{32}^2}{x_{32}^2} Q_{32}(z''). \tag{110}$$

C. Evolution equations at large N_c and N_f

Combining all the above results we write the small-x helicity evolution equations in the large-N_c and N_f limit:

$$Q_{10}(z) = Q_{10}^{(0)}(z) + \frac{\alpha_s N_c}{2\pi} \int_{\frac{\Lambda^2}{s}}^{z} \frac{dz'}{z'} \int_{1/(z's)}^{x_{10}^2} \frac{dx_{21}^2}{x_{21}^2} \left\{ \frac{1}{2} \Gamma_{10,21}^{\mathrm{adj}}(z') + \frac{1}{2} G_{21}^{\mathrm{adj}}(z') + Q_{21}(z') - \bar{\Gamma}_{10,21}(z') \right\}$$
$$+ \frac{\alpha_s N_c}{4\pi} \int_{\Lambda^2/s}^{z} \frac{dz'}{z'} \int_{1/(z's)}^{x_{10}^2 z/z'} \frac{dx_{21}^2}{x_{21}^2} Q_{21}(z'), \tag{111a}$$

$$G_{10}^{\mathrm{adj}}(z) = G_{10}^{\mathrm{adj}(0)}(z) + \frac{\alpha_s N_c}{2\pi} \int_{\max\{\Lambda^2, 1/x_{10}^2\}/s}^{z} \frac{dz'}{z'} \int_{1/(z's)}^{x_{10}^2} \frac{dx_{21}^2}{x_{21}^2} [\Gamma_{10,21}^{\mathrm{adj}}(z') + 3 G_{21}^{\mathrm{adj}}(z')]$$
$$- \frac{\alpha_s N_f}{2\pi} \int_{\Lambda^2/s}^{z} \frac{dz'}{z'} \int_{1/(z's)}^{x_{10}^2 z/z'} \frac{dx_{21}^2}{x_{21}^2} \bar{\Gamma}_{10;21}^{\mathrm{gen}}(z'), \tag{111b}$$

$$\Gamma_{10,21}^{\mathrm{adj}}(z') = \Gamma_{10,21}^{\mathrm{adj}(0)}(z') + \frac{\alpha_s N_c}{2\pi} \int_{\max\{\Lambda^2, 1/x_{10}^2\}/s}^{z'} \frac{dz''}{z''} \int_{1/(z''s)}^{\min\{x_{10}^2, x_{21}^2 z'/z''\}} \frac{dx_{32}^2}{x_{32}^2} [\Gamma_{10,32}^{\mathrm{adj}}(z'') + 3 G_{32}^{\mathrm{adj}}(z'')]$$
$$- \frac{\alpha_s N_f}{2\pi} \int_{\Lambda^2/s}^{z'} \frac{dz''}{z''} \int_{1/(z''s)}^{x_{21}^2 z'/z''} \frac{dx_{32}^2}{x_{32}^2} \bar{\Gamma}_{10;32}^{\mathrm{gen}}(z''), \tag{111c}$$

$$\bar{\Gamma}_{10,21}(z') = \bar{\Gamma}_{10,21}^{(0)}(z') + \frac{\alpha_s N_c}{2\pi} \int_{\frac{\Lambda^2}{s}}^{z'} \frac{dz''}{z''} \int_{1/(z''s)}^{\min\{x_{10}^2, x_{21}^2 z'/z''\}} \frac{dx_{32}^2}{x_{32}^2} \left\{ \frac{1}{2} \Gamma_{10,32}^{\mathrm{adj}}(z'') + \frac{1}{2} G_{32}^{\mathrm{adj}}(z'') + Q_{32}(z'') - \bar{\Gamma}_{10,32}(z'') \right\}$$
$$+ \frac{\alpha_s N_c}{4\pi} \int_{\Lambda^2/s}^{z'} \frac{dz''}{z''} \int_{1/(z''s)}^{x_{21}^2 z/z'} \frac{dx_{32}^2}{x_{32}^2} Q_{32}(z''). \tag{111d}$$

These equations have to be compared to Eqs. (92) and (93) in [9], while realizing that $A = Q$ there. Writing

$$G^{\mathrm{adj}} = 2 G^{\mathrm{old}}, \qquad \Gamma^{\mathrm{adj}} = 2 \Gamma^{\mathrm{old}} \tag{112}$$

with the $G^{\mathrm{old}}, \Gamma^{\mathrm{old}}$ denoting the objects used in Eqs. (92) and (93) of [9], we almost reduce Eqs. (111) to Eqs. (92) and (93) of [9]. The only remaining difference is due to $\bar{\Gamma}^{\mathrm{gen}}$ used in Eqs. (111b) and (111c) while only $\bar{\Gamma}$ entered in the similar place in the analogous equations of [9]. We believe that our present use of $\bar{\Gamma}^{\mathrm{gen}}$ corrects this inaccuracy done in our earlier work.

VI. CONCLUSIONS

In this paper we have presented a completely operator-based approach to helicity evolution at small x. For the first time ever we have derived explicit expressions for the fundamental and adjoint polarized Wilson lines, given in Eqs. (51) and (64) respectively. Employing these expressions, we have rederived the small-x evolution equations for

the polarized dipole amplitudes in the double logarithmic approximation, arriving at Eqs. (77) and (78) in the large-N_c limit and at Eqs. (111) in the large-N_c and N_f limits. These equations had previously been derived in [9] using a combination of the operator-based and diagrammatic methods; Eqs. (111) contain a minor correction for their prototype in [9].

As mentioned in the Introduction, the large-N_c helicity evolution equations (77) and (78) were solved in our earlier works, both numerically [10] and analytically [12], resulting in the quark helicity asymptotics given in Eq. (1). The large-N_c and N_f equations (111) have not been solved yet. Note that, on general grounds, one expects the large-N_c and N_f equations to be more realistic than the large-N_c ones, since the former include the true quark contribution, in addition to the gluon one. Hence we believe solution of the (presently corrected) large-N_c and N_f helicity evolution equations would represent an important next step in our theoretical understanding of quark helicity at small x.

Another important future research direction which may result from the present work is the possibility of obtaining the helicity analogue of JIMWLK evolution, possibly following the method outlined in [66] for rederiving the original unpolarized JIMWLK evolution starting from the evolution of Wilson lines. Obtaining a helicity JIMWLK equation may allow one to numerically determine the small-x asymptotics of quark (and possibly gluon) helicity distributions outside the large-N_c and large-N_c and N_f limits addressed above and in [9–13]. In addition, the evolution of higher-order (beyond-dipole amplitude) correlators, such as color-quadrupoles, sextupoles, etc., including exactly one polarized Wilson line may be derived using helicity JIMWLK evolution.

Finally, while the discussion in this work is dedicated to small-x helicity evolution only, the operator techniques we develop here can be used to determine the small-x asymptotics of other TMDs. The prescription remains the same as above (see also [13]):

(i) Start with the operator definition of a given TMD and simplify it in the small-x limit.

(ii) For quark distribution this results in expressing the TMDs in terms of the polarized Wilson lines, the exact expressions for which have to be determined in a separate calculation. For gluon distribution, the explicit form of the corresponding polarized Wilson lines emerges explicitly from the simplification of the operator definition at small x [13]. (The polarized Wilson lines entering the expressions for the quark and gluon distributions at small x were different in the case of helicity, and not only by the color representation factors [13]: it is natural to expect that the difference will persist for other spin-dependent quark and gluon TMDs.)

(iii) Construct the small-x evolution of the polarized dipole operators made out of the obtained fundamental and adjoint polarized Wilson lines. The evolution may start in the DLA limit, if it applies for a given TMD, and continue with the LLA corrections and beyond. Otherwise the evolution may start in the LLA limit, as is the case for unpolarized distributions. (At higher orders impact factors have to be included as well.) The equations are likely to close in the large-N_c and large-N_c and N_f limits only.

(iv) Solve the obtained equations, either numerically or, if possible, analytically, to obtain the small-x asymptotics of the TMD in question.

Application of this prescription to the quark transversity distribution is under way and will be reported on shortly [43].

ACKNOWLEDGMENTS

APPENDIX A: DIAGRAMS A AND E CANCELLATION

The one-gluon contributions to the diagrams A and E are shown in the top row of Fig. 10, where instead of the diagram E we are showing it mirror image.

We begin by evaluating the contribution to the diagram A in Fig. 10. There we only need to evaluate the contribution of the Wilson lines. Working in the $A^- = 0$ gauge we write for the Wilson line contribution, mainly arising from the "++" component of the gluon propagator,

$$(ig)(-ig)C_F \int_0^\infty dx_1^- dx_2^- e^{-\epsilon(x_1^- + x_2^-)}$$

$$\times \int \frac{d^4 q}{(2\pi)^4} e^{-iq^+(x_2^- - x_1^-) - i\underline{q}\cdot(\underline{\zeta} - \underline{\xi})} (2\pi)\delta^{(+)}(q^2) \frac{2q^+}{q^-}$$

$$= \frac{2\alpha_s C_F}{\pi} Y \ln \frac{1}{|\underline{\zeta} - \underline{\xi}|\Lambda}, \tag{A1}$$

where we have replaced

$$\int_0^\infty \frac{dq^-}{q^-} \to Y, \tag{A2}$$
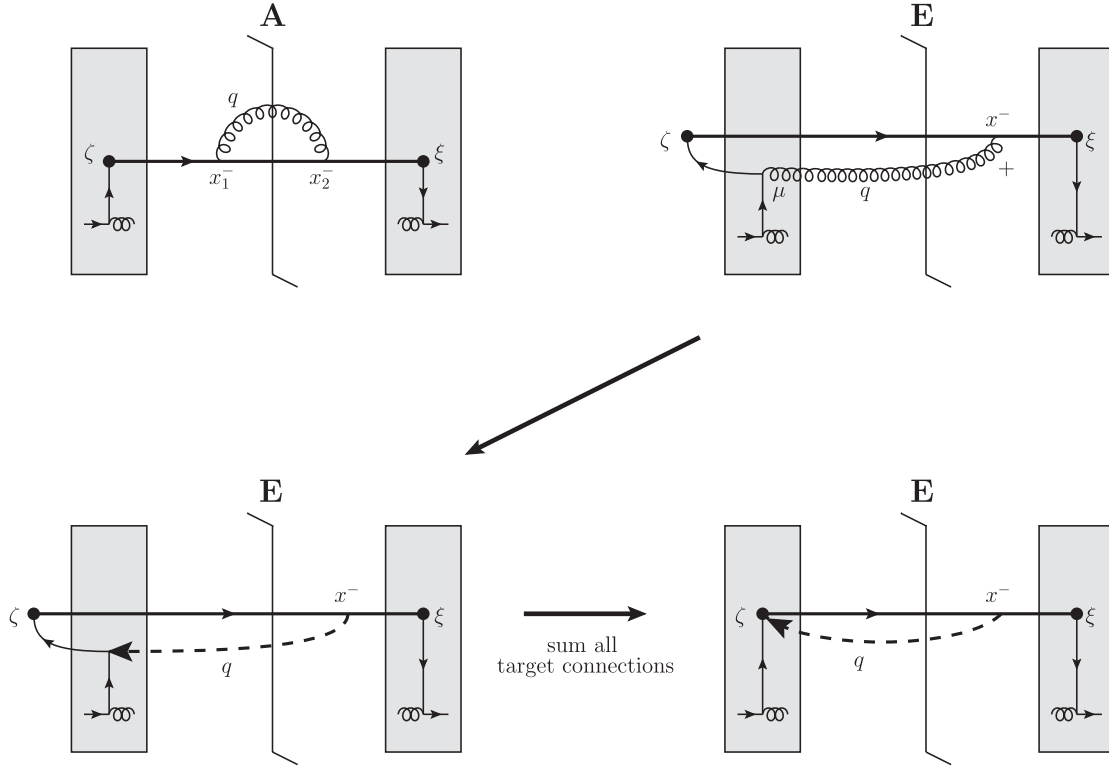
FIG. 10.   Top row: one-gluon corrections to the diagrams A and E. Bottom row: the leading (DLA) part of the diagram E comes with the longitudinally polarized contribution to the gluon propagator, denoted by the dashed line with the arrow at the end following [67,68]. The diagram in the right panel of the bottom row results from adding to the left bottom-row diagrams all the graphs with all other possible arrow-end of the dashed line connections to the shock wave.

as expected when the q^--integral is properly regularized (Y is the rapidity variable). In Eq. (A1) we have also included exponential regulators for the x^- integrals [69]. With the help of Eqs. (A1) and (8) we arrive at the following contribution of the diagram A in Fig. 10:

$$A = \frac{2p^+}{(2\pi)^3} \int d^2\zeta d\zeta^- d^2\xi d\xi^- e^{ik\cdot(\zeta-\xi)} \left\langle \bar{\psi}(\xi) \frac{1}{2}\gamma^+\gamma^5\psi(\zeta) \right\rangle$$

$$\times \frac{2\alpha_s C_F}{\pi} Y \ln \frac{1}{|\underline{\zeta}-\underline{\xi}|\Lambda}. \qquad (A3)$$

To evaluate the diagrams in the E-class, first let us note that the contribution of the Wilson line and the gluon propagator is proportional to

$$\int_0^\infty dx^- e^{-iq^+x^- -\epsilon x^-} (2\pi)\delta^{(+)}(q^2) D^{\mu+}(q)$$

$$= (2\pi)\delta^{(+)}(q^2) \left[-g^{\mu+} + \frac{q^\mu + q^+\bar{\eta}^\mu}{q^-} \right] \frac{-i}{q^+ - i\epsilon} \qquad (A4)$$

where $\bar{\eta}^\mu = (1, 0, \underline{0})$ in the $(+, -, \perp)$ notation. To obtain a logarithm of energy, we need to have $1/q^-$; hence, the $g^{\mu+}$ term in Eq. (A4) can be discarded. Since $\bar{\eta} \cdot v = v^-$ for any 4-vector v^μ, one can show that the term in Eq. (A4)

containing $\bar{\eta}^\mu$ would lead to a power of the minus momentum of the target proton, which is very small (for the plus-moving proton that we have). Hence this term can also be discarded. We are left with

$$(2\pi)\delta^{(+)}(q^2) \left[\frac{q^\mu}{q^-} \right] \frac{-i}{q^+ - i\epsilon}. \qquad (A5)$$

The transition from Eq. (A4) to Eq. (A5) is illustrated in the left panel of the second row of Fig. 10, where the gluon line is replaced by a dashed line with the arrow indicating the end of the dashed line corresponding to the q^μ factor in the part of the propagator left in Eq. (A5). This is the standard convention for the gluon lines with a longitudinal polarization on one end that is used to diagrammatically illustrate the Ward identity in QCD [67,68].

To apply the Ward identity we need to add the diagrams where the dashed line connects (with the arrow end) to the rest of the shock wave in the amplitude. This application of the Ward identity is pictured in Fig. 11; summing over all the E-class diagrams where the gluon connects to parts of the target, we arrive at the contribution graphically depicted in the lower-right panel of Fig. 10 in the notation of [67,68]. This means that the field $\psi(\zeta)$ remains intact. We thus obtain for the contribution of the E-class diagrams considered here
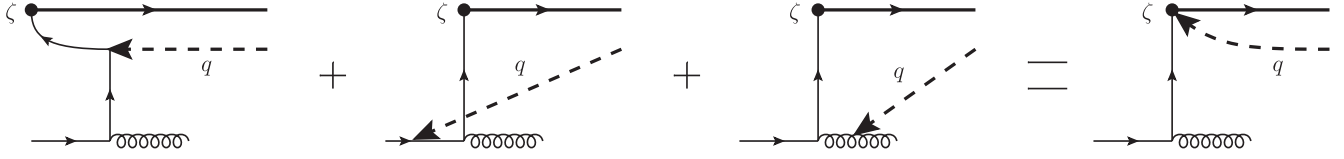
FIG. 11.   Application of the Ward identity to the diagrams in the E-class. We only depict the amplitude of the diagram; the complex conjugate amplitude remains the same for all graphs.

$$E + \cdots = \frac{2p^+}{(2\pi)^3} \int d^2\zeta d\zeta^- d^2\xi d\xi^- e^{ik\cdot(\zeta-\xi)} \langle \bar{\psi}(\xi) \frac{1}{2}\gamma^+\gamma^5 \psi(\zeta)\rangle (ig)(-ig)(-i)C_F$$
$$\times \int \frac{d^4q}{(2\pi)^4} e^{-i\underline{q}\cdot(\underline{\zeta}-\underline{\xi})} (2\pi)\delta^{(+)}(q^2) \frac{1}{q^-} \frac{-i}{q^+ - i\epsilon}. \tag{A6}$$

The additional factor of $-i$ arises due to Ward identity. Performing all the q integrals in Eq. (A6) we arrive at

$$E + \cdots = -\frac{2p^+}{(2\pi)^3} \int d^2\zeta d\zeta^- d^2\xi d\xi^- e^{ik\cdot(\zeta-\xi)} \langle \bar{\psi}(\xi) \frac{1}{2}\gamma^+\gamma^5 \psi(\zeta)\rangle \frac{\alpha_s C_F}{\pi} Y \ln \frac{1}{|\underline{\zeta}-\underline{\xi}|\Lambda} = -\frac{A}{2}. \tag{A7}$$

We conclude that the E-class diagrams cancel the diagram A. The other half of A is canceled by the complex conjugate of the diagram E in Fig. 10.[5]

The calculation can be repeated with the same conclusion for the A-type diagram where the gluon line begins and ends on the same Wilson line, say the line that begins at ζ in Fig. 10. In this case we would consider the E-type diagrams with the gluon (dashed) line Fig. 10 that does not cross the final-state cut, and is emitted by the same Wilson line originating at ζ. The A-type diagram with the gluon line beginning and ending on the same Wilson line has an extra symmetry factor of $1/2$, ensuring the exact cancellation.

Similar cancellation of diagrams A, E, and C is likely to be valid at higher orders in α_s and at LLA in $1/x$, by successive application of Ward identity.

APPENDIX B: POLARIZED DIPOLE AMPLITUDES AT BORN LEVEL

Let us compare the calculation of the initial conditions for the flavor singlet and nonsinglet polarized dipole amplitudes defined above in Eqs. (28) and (35) to what was done in [11]. For simplicity we will focus on the t-channel quark exchanges: the exchanges of t-channel gluons can be done similarly.

1. Flavor-singlet case

(i) First consider the definition in Eq. (28). Assuming that the target is a single quark, the flavor-singlet quark helicity TMD is proportional to

$$\mathrm{Re}\, \langle q| \mathrm{T}\, \mathrm{tr} \left[V_0\, V_1^{pol,\dagger} \right] |q\rangle + \mathrm{Re}\, \langle q| \mathrm{T}\, \mathrm{tr} \left[V_1^{pol}\, V_0^{\dagger} \right] |q\rangle = -\frac{1}{2} \quad \text{}, \tag{B1}$$
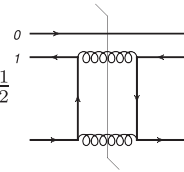
in agreement with Eq. (10) of [11].

(ii) Now let us try to see what this result means for uncut diagrams. Again assume that the target is a quark. Furthermore, note that the matrix element of the Wilson lines gives us an expectation value of an S-matrix (or, for the problem at hand, its spin-dependent part), which is given by iM with M the scattering amplitude. That is,

$$i\,M \equiv \langle q| \mathrm{T}\, \mathrm{tr} \left[V_0\, V_1^{pol,\dagger} \right] |q\rangle = \quad \text{}. \tag{B2}$$

---
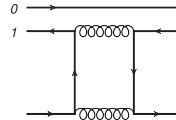
[5]The cancellation demonstrated here assumes that the range of q^- integrals is the same in the diagrams A and E: while this is correct in the leading logarithmic approximation in x, it is not true beyond the small-x approximation, where large logarithms of Q^2 are generated in the sum of A and E diagrams [70], contributing to the Sudakov form factor. Here we assume that Q^2 is not large enough to require a separate resummation of $\ln Q^2$.

[Only the first term in Eq. (B1) has a real part for t-channel quark exchanges we are restricting ourselves to; hence we will only keep this term in the short exercise below.]

We see that

$$\mathrm{Re}[i\,M] = -\mathrm{Im}M = \tfrac{1}{2}[i\,M + (i\,M)^*] = \tfrac{1}{2}\,\langle q|\,\mathrm{T\,tr}\left[V_0\,V_1^{pol,\,\dagger}\right]|q\rangle + \tfrac{1}{2}\,\langle q|\,\overline{\mathrm{T}}\,\mathrm{tr}\left[V_1^{pol}\,V_0^{\dagger}\right]|q\rangle$$
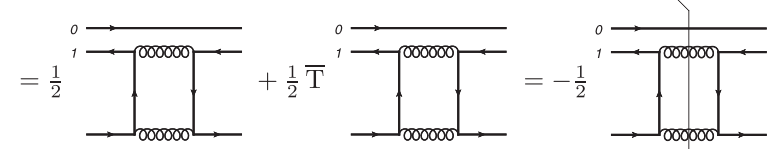
$$= \tfrac{1}{2}\;\;\;\; + \tfrac{1}{2}\,\overline{\mathrm{T}}\;\;\;\; = -\tfrac{1}{2}\;\;\;\;. \tag{B3}$$

Note that under the antitime ordering $\overline{\mathrm{T}}$ the "regular" Wilson line, say V_1, denotes a quark (particle number flows in the same direction as the new time), which for the normal-flowing time would appear as an anti-quark; similarly the conjugate Wilson line $V_0^\dagger$ denotes an anti-quark, but appears to be a quark for the normal-flowing time. The target quark state $|q\rangle$ can be thought of as an antiquark under $\overline{\mathrm{T}}$, since the particle number flows opposite to the new time: if we represent it by another Wilson line operator in the amplitude, it would conjugate in the cc amplitude, giving an antiquark. Hence, the second diagram in the second line of Eq. (B3) looks just like the first diagram, only time in the second diagram flows in the opposite direction, as indicated by $\overline{\mathrm{T}}$. In other word, the $\overline{\mathrm{T}}$

sign means that the diagram is to the right of an (imaginary) final-state cut (that is, in the complex conjugate amplitude).

Note that each diagram corresponds to iM, such that

$$iM + (iM)^* = \mathrm{Diagram} + \mathrm{Diagram}^*. \tag{B4}$$

Again, only the Im part of the amplitude contributes in Eq. (B3).

2. Flavor nonsinglet case

(iii) Let us now consider the flavor nonsinglet case. As follows from Eq. (35), the corresponding TMD is proportional to the real part of following operator expectation value [11] (again for a quark target)
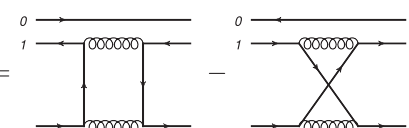
$$\langle q|\mathrm{T\,tr}\left[V_0\,V_1^{pol,\,\dagger}\right]|q\rangle - \langle q|\mathrm{T\,tr}\left[V_1^{pol}\,V_0^{\dagger}\right]|q\rangle = \;\;\;\; - \;\;\;\;. \tag{B5}$$

Now, the second diagram contributes no imaginary part to the scattering amplitude. Its real part contribution can be related to the following diagram due to the crossing symmetry:
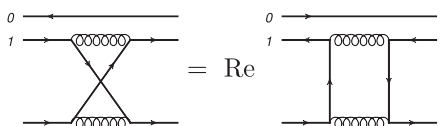
 $= \mathrm{Re}$. (B6)

Here we assume that the corresponding amplitude in Eq. (B2) is of the type $M(s,t) = f(t)(\ln(s/t) \pm i\pi)^2 + \mathcal{O}(1/s)$, as expected for the helicity-dependent quark exchange at the sub-eikonal level. Then the amplitude on the left of Eq. (B6) is $M_{\mathrm{crossed}}(s,t) = M(u,t)$ with

$u < 0$. At high energy $u \approx -s$ such that $M_{\mathrm{crossed}}(s,t) = \mathrm{Re}M_{\mathrm{crossed}}(s,t) = \mathrm{Re}M(-s,t) = \mathrm{Re}M(s,t)$ for the leading DLA part of our ansatz for the amplitude $M(s,t)$, which is what is implied in the diagrammatic equality Eq. (B6).

The Re sign in Eq. (B6) applies to the amplitude M, rather than to the diagram, which is iM, such that
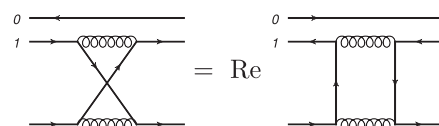
 $= \mathrm{Re}$ $= i\,\mathrm{Re}M.$ (B7)

We conclude that

$$\langle q|\mathrm{T}\,\mathrm{tr}\left[V_0\,V_1^{pol,\,\dagger}\right]|q\rangle - \langle q|\mathrm{T}\,\mathrm{tr}\left[V_1^{pol}\,V_0^{\dagger}\right]|q\rangle = \quad\raisebox{-1em}{\includegraphics{diagram}}\quad = i\,M - i\,\mathrm{Re}M = -\mathrm{Im}M. \quad \text{(B8)}$$

This result is in agreement with Eq. (56) of [11]. In addition, the expectation value of the operator from Eq. (35) is real, thus justifying the assumption made in [11].

[1] A. Accardi, J. Albacete, M. Anselmino, N. Armesto, E. Aschenauer *et al.*, Electron ion collider: The next QCD frontier—Understanding the glue that binds us all, Eur. Phys. J. A **52**, 268 (2016).

[2] E. C. Aschenauer *et al.*, The RHIC spin program: Achievements and future opportunities, arXiv:1304.0079.

[3] E.-C. Aschenauer *et al.*, The RHIC SPIN program: Achievements and future opportunities, arXiv:1501.01220.

[4] E.-C. Aschenauer *et al.*, The RHIC cold QCD plan for 2017 to 2023: A portal to the EIC, arXiv:1602.03922.

[5] R. L. Jaffe and A. Manohar, The G(1) problem: Fact and fantasy on the spin of the proton, Nucl. Phys. **B337**, 509 (1990).

[6] X.-D. Ji, Gauge-Invariant Decomposition of Nucleon Spin, Phys. Rev. Lett. **78**, 610 (1997).

[7] X. Ji, X. Xiong, and F. Yuan, Proton Spin Structure from Measurable Parton Distributions, Phys. Rev. Lett. **109**, 152005 (2012).

[8] E. Leader and C. Lorce, The angular momentum controversy: What's it all about and does it matter?, Phys. Rep. **541**, 163 (2014).

[9] Y. V. Kovchegov, D. Pitonyak, and M. D. Sievert, Helicity evolution at small-x, J. High Energy Phys. 01 (2016) 072.

[10] Y. V. Kovchegov, D. Pitonyak, and M. D. Sievert, Small-x Asymptotics of the Quark Helicity Distribution, Phys. Rev. Lett. **118**, 052001 (2017).

[11] Y. V. Kovchegov, D. Pitonyak, and M. D. Sievert, Helicity evolution at small x: Flavor singlet and non-singlet observables, Phys. Rev. D **95**, 014033 (2017).

[12] Y. V. Kovchegov, D. Pitonyak, and M. D. Sievert, Small-x asymptotics of the quark helicity distribution: Analytic results, Phys. Lett. B **772**, 136 (2017).

[13] Y. V. Kovchegov, D. Pitonyak, and M. D. Sievert, Small-x asymptotics of the gluon helicity distribution, J. High Energy Phys. 10 (2017) 198.

[14] J. Bartels, B. Ermolaev, and M. Ryskin, Nonsinglet contributions to the structure function g1 at small x, Z. Phys. C **70**, 273 (1996).

[15] J. Bartels, B. Ermolaev, and M. Ryskin, Flavor singlet contribution to the structure function G(1) at small x, Z. Phys. C **72**, 627 (1996).

[16] R. Kirschner and L. Lipatov, Double logarithmic asymptotics and Regge singularities of quark amplitudes with flavor exchange, Nucl. Phys. **B213**, 122 (1983).

[17] R. Kirschner, Regge asymptotics of scattering amplitudes in the logarithmic approximation of QCD, Z. Phys. C **31**, 135 (1986).

[18] R. Kirschner, Regge asymptotics of scattering with flavor exchange in QCD, Z. Phys. C **67**, 459 (1995).

[19] R. Kirschner, Reggeon interactions in perturbative QCD, Z. Phys. C **65**, 505 (1995).

[20] S. Griffiths and D. Ross, Studying the perturbative Reggeon, Eur. Phys. J. C **12**, 277 (2000).

[21] K. Itakura, Y. V. Kovchegov, L. McLerran, and D. Teaney, Baryon stopping and valence quark distribution at small x, Nucl. Phys. **A730**, 160 (2004).

[22] J. Bartels and M. Lublinsky, Quark anti-quark exchange in $\gamma^*\gamma^*$ scattering, J. High Energy Phys. 09 (2003) 076.

[23] E. A. Kuraev, L. N. Lipatov, and V. S. Fadin, The Pomeranchuk singlularity in non-Abelian gauge theories, Sov. Phys. JETP **45**, 199 (1977).

[24] I. Balitsky and L. Lipatov, The Pomeranchuk singularity in quantum Chromodynamics, Sov. J. Nucl. Phys. **28**, 822 (1978).

[25] I. Balitsky, Operator expansion for high-energy scattering, Nucl. Phys. **B463**, 99 (1996).

[26] I. Balitsky, Factorization and high-energy effective action, Phys. Rev. D **60**, 014020 (1999).

[27] Y. V. Kovchegov, Small-x F_2 structure function of a nucleus including multiple pomeron exchanges, Phys. Rev. D **60**, 034008 (1999).

[28] Y. V. Kovchegov, Unitarization of the BFKL pomeron on a nucleus, Phys. Rev. D **61**, 074018 (2000).

[29] J. Jalilian-Marian, A. Kovner, and H. Weigert, The Wilson renormalization group for low x physics: Gluon evolution at finite parton density, Phys. Rev. D **59**, 014015 (1998).

[30] J. Jalilian-Marian, A. Kovner, A. Leonidov, and H. Weigert, The Wilson renormalization group for low x physics: Towards the high density regime, Phys. Rev. D **59**, 014014 (1998).

[31] E. Iancu, A. Leonidov, and L. D. McLerran, The renormalization group equation for the color glass condensate, Phys. Lett. B **510**, 133 (2001).

[32] E. Iancu, A. Leonidov, and L. D. McLerran, Nonlinear gluon evolution in the color glass condensate. I, Nucl. Phys. **A692**, 583 (2001).

[33] Y. Hatta, Y. Nakagawa, F. Yuan, Y. Zhao, and B. Xiao, Gluon orbital angular momentum at small-x, Phys. Rev. D **95**, 114032 (2017).

[34] T. Altinoluk, N. Armesto, G. Beuf, M. Martinez, and C. A. Salgado, Next-to-eikonal corrections in the CGC: Gluon production and spin asymmetries in pA collisions, arXiv:1404.2219.

[35] J. Jalilian-Marian, Elastic scattering of a quark from a color field: longitudinal momentum exchange, Phys. Rev. D **96**, 074020 (2017).

[36] G. A. Chirilli, Sub-eikonal corrections to scattering amplitudes at high energy, J. High Energy Phys. 01 (2019) 118.

[37] I. Balitsky and A. Tarasov, Rapidity evolution of gluon TMD from low to moderate x, J. High Energy Phys. 10 (2015) 017.

[38] I. Balitsky and A. Tarasov, Gluon TMD in particle production from low to moderate x, J. High Energy Phys. 06 (2016) 164.

[39] A. Metz and J. Zhou, Distribution of linearly polarized gluons inside a large nucleus, Phys. Rev. D **84**, 051503 (2011).

[40] A. Dumitru and V. Skokov, Anisotropy of the semiclassical gluon field of a large nucleus at high energy, Phys. Rev. D **91**, 074006 (2015).

[41] D. Boer, S. Cotogno, T. van Daal, P. J. Mulders, A. Signori, and Y.-J. Zhou, Gluon and Wilson loop TMDs for hadrons of spin ≤ 1, J. High Energy Phys. 10 (2016) 013.

[42] C. Marquet, C. Roiesnel, and P. Taels, Linearly polarized small-x gluons in forward heavy-quark pair production, Phys. Rev. D **97**, 014004 (2018).

[43] Y. V. Kovchegov and M. D. Sievert, Valence quark transversity at small x, Phys. Rev. D **99**, 054033 (2019).

[44] P. J. Mulders and R. D. Tangerman, The complete tree level result up to order 1/Q for polarized deep inelastic leptoproduction, Nucl. Phys. **B461**, 197 (1996).

[45] L. V. Gribov, E. M. Levin, and M. G. Ryskin, Semihard processes in QCD, Phys. Rep. **100**, 1 (1983).

[46] A. H. Mueller and J.-w. Qiu, Gluon recombination and shadowing at small values of x, Nucl. Phys. **B268**, 427 (1986).

[47] L. D. McLerran and R. Venugopalan, Computing quark and gluon distribution functions for very large nuclei, Phys. Rev. D **49**, 2233 (1994).

[48] L. D. McLerran and R. Venugopalan, Gluon distribution functions for very large nuclei at small transverse momentum, Phys. Rev. D **49**, 3352 (1994).

[49] L. D. McLerran and R. Venugopalan, Green's functions in the color field of a large nucleus, Phys. Rev. D **50**, 2225 (1994).

[50] Y. V. Kovchegov, Non-abelian Weizsäcker-Williams field and a two-dimensional effective color charge density for a very large nucleus, Phys. Rev. D **54**, 5463 (1996).

[51] Y. V. Kovchegov, Quantum structure of the non-Abelian Weizsäcker-Williams field for a very large nucleus, Phys. Rev. D **55**, 5445 (1997).

[52] J. Jalilian-Marian, A. Kovner, L. D. McLerran, and H. Weigert, The intrinsic glue distribution at very small x, Phys. Rev. D **55**, 5414 (1997).

[53] E. Iancu and R. Venugopalan, The color glass condensate and high energy scattering in QCD, arXiv:hep-ph/0303204, DOI: 10.1142/9789812795533_0005.

[54] H. Weigert, Evolution at small x_{bj}: The color glass condensate, Prog. Part. Nucl. Phys. **55**, 461 (2005).

[55] J. Jalilian-Marian and Y. V. Kovchegov, Saturation physics and deuteron gold collisions at RHIC, Prog. Part. Nucl. Phys. **56**, 104 (2006).

[56] F. Gelis, E. Iancu, J. Jalilian-Marian, and R. Venugopalan, The color glass condensate, Annu. Rev. Nucl. Part. Sci. **60**, 463 (2010).

[57] J. L. Albacete and C. Marquet, Gluon saturation and initial conditions for relativistic heavy ion collisions, Prog. Part. Nucl. Phys. **76**, 1 (2014).

[58] Y. V. Kovchegov and E. Levin, *Quantum Chromodynamics at High Energy* (Cambridge University Press, Cambridge, England, 2012).

[59] Y. V. Kovchegov and M. D. Sievert, Calculating TMDs of a large nucleus: Quasi-classical approximation and quantum evolution, Nucl. Phys. **B903**, 164 (2016).

[60] G. P. Lepage and S. J. Brodsky, Exclusive processes in perturbative quantum chromodynamics, Phys. Rev. D **22**, 2157 (1980).

[61] Y. V. Kovchegov and K. Tuchin, Inclusive gluon production in DIS at high parton density, Phys. Rev. D **65**, 074026 (2002).

[62] A. Mueller and S. Munier, $p_\perp$-broadening and production processes versus dipole/quadrupole amplitudes at next-to-leading order, Nucl. Phys. **A893**, 43 (2012).

[63] Y. V. Kovchegov, L. Szymanowski, and S. Wallon, Perturbative odderon in the dipole model, Phys. Lett. B **586**, 267 (2004).

[64] Y. Hatta, E. Iancu, K. Itakura, and L. McLerran, Odderon in the color glass condensate, Nucl. Phys. **A760**, 172 (2005).

[65] Y. V. Kovchegov and M. D. Sievert, A new mechanism for generating a single transverse spin asymmetry, Phys. Rev. D **86**, 034028 (2012).

[66] A. H. Mueller, A Simple derivation of the JIMWLK equation, Phys. Lett. B **523**, 243 (2001).

[67] G. 't Hooft, Renormalizable Lagrangians for Massive Yang-Mills Fields, Nucl. Phys. **B35**, 167 (1971).

[68] G. Sterman, *An Introduction to Quantum Field Theory* (Cambridge University Press, Cambridge, England, 1993).

[69] G. A. Chirilli, Y. V. Kovchegov, and D. E. Wertepny, Classical gluon production amplitude for nucleus-nucleus collisions: First saturation correction in the projectile, J. High Energy Phys. 03 (2015) 015.

[70] A. H. Mueller, B. Wu, B.-W. Xiao, and F. Yuan, Medium induced transverse momentum broadening in hard processes, Phys. Rev. D **95**, 034007 (2017).